Precambrian Research 393 (2023) 107104

Contents lists available at ScienceDirect

Precambrian Research

journal homepage: www.elsevier.com/locate/precamres

New record of the green algal fossil *Proterocladus* and coexisting microfossils from the Meso-Neoproterozoic Diaoyutai Formation in southern Liaoning, North China

Dongdong Li [a], Genming Luo [a,*], Qing Tang [b,c], Zhenbing She [a], Shuhai Xiao [d]

[a] State Key Laboratory of Biogeology and Environmental Geology, and School of Earth Sciences, China University of Geosciences, Wuhan 430074, China
[b] State Key Laboratory for Mineral Deposits Research, School of Earth Sciences and Engineering, and Frontiers Science Center for Critical Earth Material Cycling, Nanjing University, Nanjing 210023, China
[c] Department of Earth Sciences, The University of Hong Kong, Pokfulam Road, Hong Kong, China
[d] Department of Geosciences and Global Change Center, Virginia Tech, Blacksburg, VA 24061, USA

ARTICLE INFO

Keywords:
Organic-walled microfossil
Proterocladus antiquus
Mesoproterozoic-Neoproterozoic
Diaoyutai Formation
North China Block

ABSTRACT

The Mesoproterozoic-Neoproterozoic transition represents a crucial interval of evolutionary innovation and phylogenetic diversification. A spotty fossil record indicates that several clades of multicellular eukaryotes, including red and green algae, as well as fungi, may have diverged and diversified at this transition. However, the Meso-Neoproterozoic fossil record remains poorly documented, particularly at the assemblage level, greatly limiting our understanding of the marine ecosystem in this critical time interval. Here we report a well-preserved assemblage of organic-walled microfossils from the Meso-Neoproterozoic Diaoyutai Formation (*ca.* 1050–950 Ma) in Southern Liaoning Province of the North China Block. Raman geothermometric analysis of these organic-walled microfossils suggests that the Diaoyutai Formation experienced relatively low-grade metamorphism, with apparent peak metamorphic temperatures of ~ 215 ℃. The Diaoyutai assemblage consists of 14 species belonging to 9 genera, as well as several unnamed or unidentified forms. In addition to simple forms such as aggregated coccoidal and unbranched filamentous fossils that are often interpreted as cyanobacteria, a moderate diversity of eukaryotes is also observed. Probable eukaryotic fossils in this assemblage include the branched multicellular alga *Proterocladus antiquus* that has been previously interpreted as a green alga, several morphologically complex spheroidal taxa (e.g., *Germinosphaera bispinosa*, *Pterospermopsimorpha insolita*, *P. pileiformis* and *Squamosphaera colonialica*), and relatively large leiospheres (50–700 μm in diameter). We note that the occurrence of *Proterocladus antiquus* in the Diaoyutai assemblage predates its previously reported occurrence from the overlying Nanfen Formation. Overall, the Diaoyutai assemblage presents a glimpse of the coastal marine ecosystem at the Meso-Neoproterozoic transition, which consisted of benthic microbial mats dominated by filamentous cyanobacteria, millimeter-sized benthic green algae with thallus elevating above the sediment–water interface, and micrometer-sized planktonic prokaryotic and eukaryotic organisms. From the perspective of primary producers, the rise of photosynthetic eukaryotes in the Meso-Neoproterozoic represents a transformative innovation to modernize the coastal marine ecosystem in terms of ecological functions.

1. Introduction

Several well-preserved organic-walled microfossils (OWMs), e.g., *Tappania*, *Shuiyousphaeridium*, *Valeria*, and *Dictyosphaera*, from the Ruyang and Changcheng groups in North China suggest that total-group eukaryotes must have diverged as early as the latest Paleoproterozoic, about 1700 Ma (Xing and Liu, 1973; Yin, 1997; Xiao et al., 1997; Lamb et al., 2009; Peng et al., 2009; Yin et al., 2020; Pang et al., 2015; Agić et al., 2015, 2017; Miao et al., 2019; Lyu et al., 2022). Many of these OWMs are also present in the early Mesoproterozoic successions (e.g., Javaux et al., 2001; Javaux and Marshal, 2006; Nagovitsin et al., 2010; Knoll, 2014; Butterfield, 2015; Javaux and Knoll, 2016; Adam et al., 2017; Sergeev et al., 2017; Shi et al., 2017; Javaux and Lepot, 2018), highlighting the generally long range of Precambrian taxa. Nonetheless,

* Corresponding author.
E-mail address: gmluo@cug.edu.cn (G. Luo).

https://doi.org/10.1016/j.precamres.2023.107104
Received 24 February 2023; Received in revised form 13 May 2023; Accepted 21 May 2023
Available online 6 June 2023

new eukaryote forms do appear in the Mesoproterozoic Era, including decimeter-sized carbonaceous compressions from the Gaoyuzhuang Formation in North China (Du et al., 1995; Zhu et al., 2016), *Rafatazmia* and *Ramathallus* from the Tirohan Dolomite of the lower Vindhyan Group in central India (Bengtson et al., 2017), and the "string-of-beads" fossil *Horodyskia* from the Appekunny Formation in western United States (Yochelson and Fedonkin, 2000; Fedonkin and Yochelson, 2002) and the Bangemall Supergroup in Western Australia (Grey and Williams, 1990; Grey et al., 2010). At the Meso-Neoproterozoic transition, eukaryotes began to expand in both taxonomic diversity and morphological disparity (Xiao and Tang, 2018). Numerous taxa of macrofossils—including *Chuaria*, *Tawuia*, *Longfengshania*, *Sinosabellidites*, *Protoarenicola*, and *Pararenicola*, which probably represent macroalgae—are widely present in the latest Mesoproterozoic through earliest Neoproterozoic strata (e.g., Hofmann, 1985; Sun et al., 1986; Han and Runnegar, 1992; Butterfield et al., 1994; Kumar, 2001; Teyssèdre, 2003; Qian et al., 2008; Tang et al., 2013, 2017, 2021; Sharma and Singh, 2019; Li et al., 2019). Of particular importance are several taxa that can be placed within the crown-group eukaryotes with confidence, including the 1050 Ma red algal fossil *Bangiomorpha pubescens* (Butterfield, 2000; Gibson et al., 2017), the 1050–950 Ma green algal fossil *Proterocladus antiquus* (Tang et al., 2020), and the ~ 1000 Ma microfossil *Arctacellularia tetragonala* that has been interpreted as a phototrophic eukaryote (Sforna et al., 2022).

The fossil record of eukaryotes is broadly consistent with molecular phylogenetic data (e.g., Yoon et al., 2004, 2010; Parfrey et al., 2011; Yang et al., 2016; Gibson et al., 2017). Most published molecular clock studies show that crown-group eukaryotes diverged no later than the Meso-Neoproterozoic transition (see Porter, 2020 for a summary). Within the crown-group eukaryotes, the origin of primary plastids (i.e., the Archaeplastida) is estimated to be ~ 1325 Ma (Yoon et al., 2004; Gibson et al., 2017; Betts et al., 2018; Evanovich and Guerreiro, 2020) or older (Strassert et al., 2021), the divergence between the Rhodophyta and Viridiplantae at ~ 1244 Ma, and the divergence of crown-group Chlorophyta at 1093 Ma (Evanovich and Guerreiro, 2020).

Although both the fossil record and molecular phylogenetic data indicate that crown-group eukaryotes diverged and diversified no later than the Meso-Neoproterozoic transition, the ecological contribution of eukaryotes to the ecosystem remains poorly documented. Organic geochemical data suggest that eukaryotes were insignificant components of the microbial community until ~ 820 Ma (e.g., Blumenberg et al., 2012; Gueneli et al., 2018; Zumberge et al., 2019). For example, hydrocarbon biomarkers from many Mesoproterozoic successions are dominated by hopanes, whereas steranes derived from eukaryotes are below the instrumental detection limit (Blumenberg et al., 2012; Luo et al., 2015, 2016; Nguyen et al., 2019). It is not until the mid-late Tonian Period when steranes become detectable and not until the late Cryogenian when the sterane/hopane ratio rises to levels above 0.5 (Brocks et al., 2017; Zumberge et al., 2019). Although taphonomic biases against sterane preservation may be responsible for the absence or low abundance of steranes in older rocks (e.g., Pawlowska et al., 2013; Porter et al., 2018; Cohen and Kodner, 2021; Eckford-Soper et al., 2022), the biomarker data are typically taken as evidence for the insignificant ecological role of eukaryotes in the microbial ecosystem (Luo et al., 2015, 2016; Nguyen et al., 2019; Zumberge et al., 2019; Zhang et al., 2021a). Alternatively, Mesoproterozoic eukaryotes were exclusively stem-group lineages that diverged before the origin of eukaryotic steroids (Porter, 2020).

To test the different hypotheses about the changing biomarker patterns across the Meso-Neoproterozoic boundary, it is important to assess the abundance of eukaryotic vs. prokaryotic fossils at the community or assemblage level. In this regard, Mesoproterozoic successions in North China (Fig. 1b) hold great promise to illuminate the early evolutionary history of eukaryotes because they host abundant microfossils that can be convincingly placed in total-group eukaryotes (e.g., Yin and Sun, 1994; Yin, 1997; Tang et al., 2013, 2015, 2020; Agić et al., 2015, 2017; Miao et al., 2019, 2021; Li et al., 2019, 2020; Han et al., 2020). Strata deposited at the Meso-Neoproterozoic transition are equally important because they contain unequivocal crown-group eukaryotes, one example of which is *Proterocladus antiquus*, which is from in the *ca.* 1050–950 Ma Nanfen Formation in Liaoning Province of North China, characterized by millimeter-sized and branched multicellular thalli, and interpreted as a benthic cladophoralean chlorophyte (Tang et al., 2020) or a total-group ulvophycean (Hou et al., 2022).

In this study, we conduct a palynological study of shales from the Diaoyutai Formation of the Xihe Group in the Fuxian District, southern Liaoning Province, North China; the Diaoyutai Formation directly underlies the Nanfen Formation from which *Proterocladus antiquus* was first reported (Tang et al., 2020). Our study reveals a microbial community consisting of abundant OWMs, including filamentous forms, spherical vesicles, and millimeter-sized algal thalli, most of which are reported for the first time from the Diaoyutai Formation. The microfossils were analyzed using light microscopy and Raman spectroscopy to characterize their morphology and thermal maturity.

2. Geological setting

Meso-Neoproterozoic successions are widespread on the eastern and southeastern margins of the North China Craton (Fig. 1), including southeastern Liaoning, eastern Jilin, western Shandong, northern Jiangsu, and northeastern Anhui provinces, collectively known as the Jiao-Liao-Xu-Huai region (e.g., Xiao et al., 1997, 2014; Qiao et al., 2001; Su, 2016; Pang et al., 2021). In southern Liaoning Province, the sequence consists of four groups—in an ascending stratigraphic order, the Yongning Group (also known as the Yongning Formation), Xihe Group, Wuhangshan Group, and Jinxian Group, which is unconformably overlain by the Dalinzi Formation of possible Cambrian age (Fig. 1d). The Yongning Group, which is mainly composed of thick-bedded conglomerates, unconformably overlies the metamorphic basement of the North China Craton. The Xihe Group, which unconformably overlies the Yongning Group and outcrops widely in the Fuxian region of southern Liaoning Province, contains three formations, which are, in an ascending stratigraphic order, the Diaoyutai, Nanfen, and Qiaotou formations.

The samples analyzed here are collected from the middle part of the Diaoyutai Formation at the Miaoshan section (GPS: 39°47.104′ N; 121°43.834′ E), which is located in the northeastern Fuxian District of Dalian City in Liaoning Province (Fig. 1c). At the Miaoshan section, the Diaoyutai Formation begins with a ~ 1 m thick conglomerate at the base (Fig. 2b) and ends with glauconitic quartz sandstones at the top, with variegated siltstone and mudstone in between (Fig. 2c–e). Among the analyzed samples, the total organic carbon (TOC) content ranges from 0.03% to 0.22%, with an average of 0.12% ($n = 17$ excluding the three samples without fossils). The lower Nanfen Formation, which overlies the Diaoyutai Formation, is mainly composed of purple-colored and thin- to medium-thick bedded fine quartz sandstone, algal limestone, and fine-grained limestone. Our field observation and previous regional geological survey suggest that the succession from the Yongning to Nanfen formations in the Fuzhou-Dalian area records a transgression sequence (LBGMR, 1989; Qiao et al., 2001). The widespread presence of cross beddings in the sandstone and horizontal beddings in the mudstone of the Diaoyutai Formation suggests that it was mainly deposited in the neritic facies (BGMR, 1989; Qiao et al., 2001; Zhang et al., 2021b).

The deposition age of the Diaoyutai Formation is constrained by numerous radiometric ages of detrital zircons and intrusive igneous rocks (Fig. 1d). The youngest detrital zircon population from the basal Yongning Group is giving an age of 1232 ± 8 Ma (e.g., Zhang et al., 2021b) and the Xingmincun Formation of the upper Jinxian Group is intruded by ~ 900 Ma diabases (Zhang et al., 2016), constraining almost the entire Meso-Neoproterozoic succession between 1232 Ma and ~ 900 Ma (Fig. 1d). Additional ages further tighten the

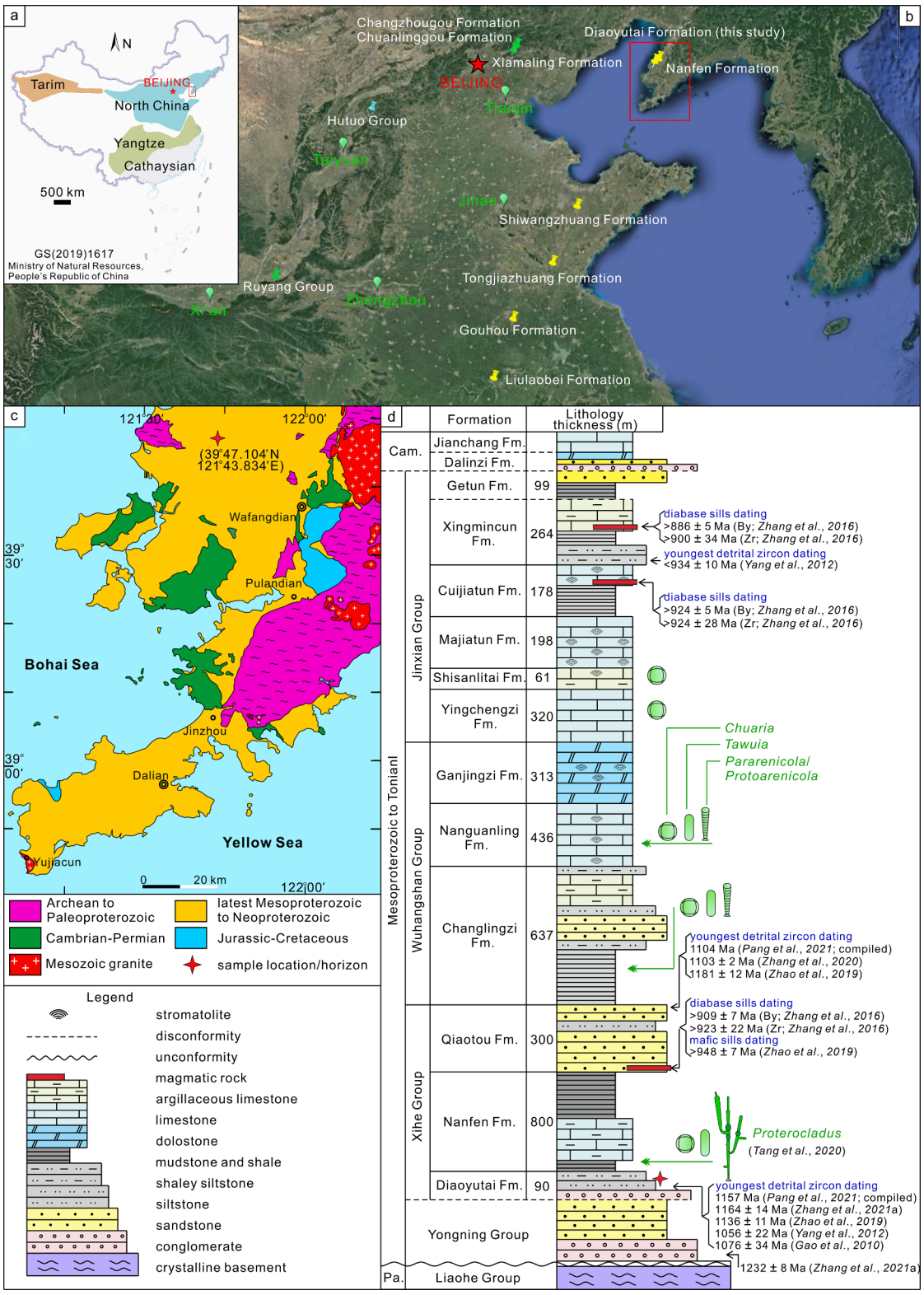

Fig. 1. Maps and stratigraphic column. (a) Location of North China Craton. (b) Google satellite panoramic image showing study area (red box) and location of key Proterozoic units that contain organic-walled microfossils. Cyan pins: Paleoproterozoic Hutuo Group (Yin et al., 2020). Green pins: Mesoproterozoic Ruyang Group (Yin, 1997; Agić et al., 2015, 2017), Changzhougou and Chuanlinggou formations (Miao et al., 2019), and Xiamaling Formation (Miao et al., 2021). Yellow pins: Meso-Neoproterozoic Shiwangzhuang Formation (Han et al., 2020; Li et al., 2020), Tongjiazhuang Formation (Li et al., 2019), Gouhou Formation (Tang et al., 2015), Liulaobei Formation (Tang et al., 2013), Nanfen Formation (Tang et al., 2020), and Diaoyutai Formation (this study). (c) Simplified geological map of southern Liaoning Province, North China. (d) Generalized stratigraphic column of Meso-Neoproterozoic strata in southern Liaoning, North China, with geochronological and paleontological data. Stratigraphic interval investigated in this study is marked by a red cross and expanded in Fig. 2a. By: baddeleyite; Zr: zircon. Geological maps and stratigraphic columns are adapted from Tang et al. (2020).

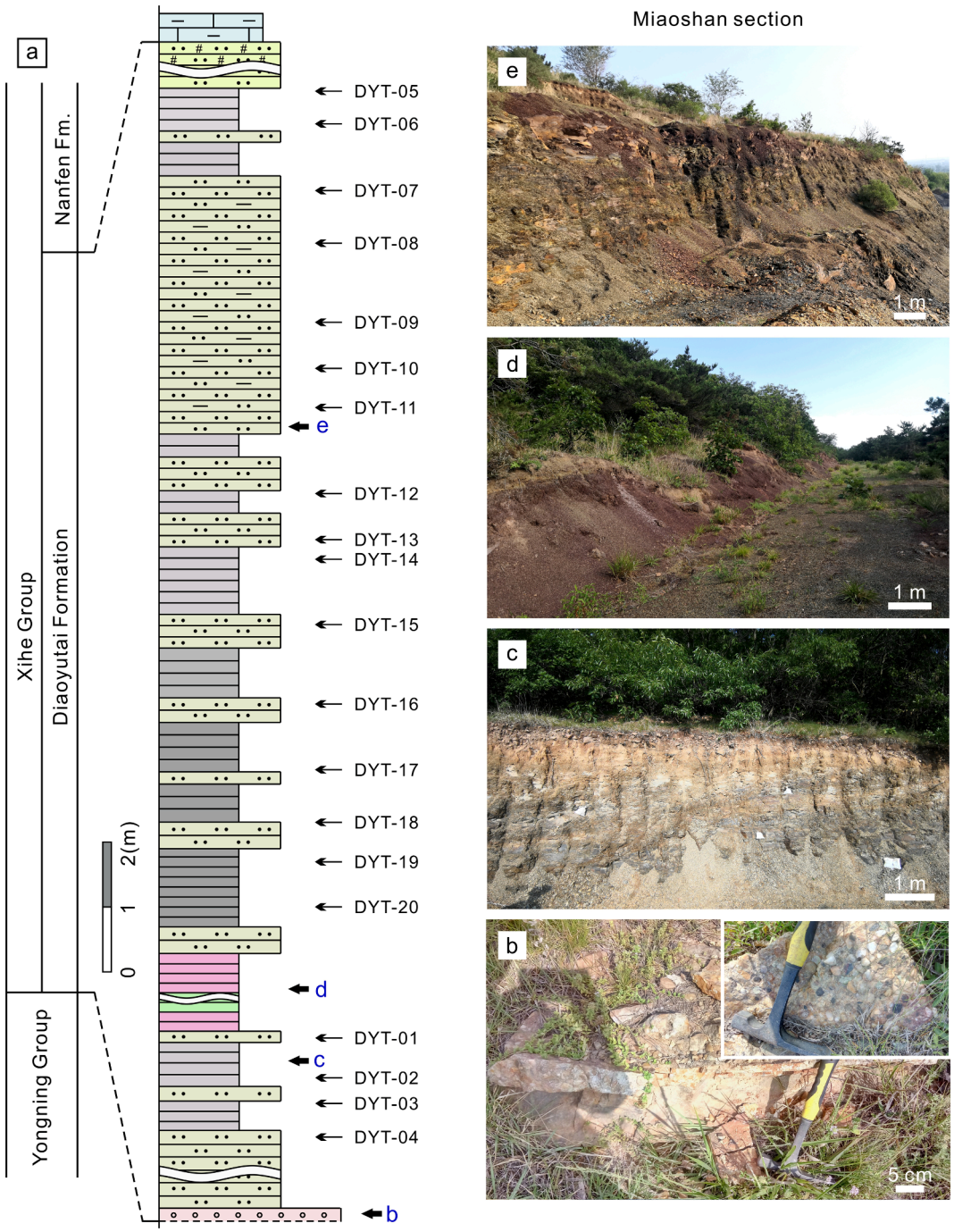

Fig. 2. Lithostratigraphic column of Diaoyutai Formation in Miaoshan area (a) and representative field photos (b–e). Long and short arrows in (a) mark, respectively, sampling horizons and approximate stratigraphic horizon of (b–e). (b) Conglomerates in basal Diaoyutai Formation, with inset showing a close-up view; (c) Gray siltstone in lower Diaoyutai Formation; (d) Maroon mudstone in middle Diaoyutai Formation; (e) Gray shale and silty shale in middle-upper Diaoyutai Formation.

geochronological constraints on the Diaoyutai Formation. For example, a diabase intruding the Qiaotou Formation, which overlies the Nanfen and Diaoyutai formations, gives an age of 948 ± 7 Ma (Zhao et al., 2019), providing a minimum age constraint on the Diaoyutai Formation. Several studies of detrital zircons from the Diaoyutai Formation suggest a maximum age constraint of ~ 1050 Ma (Gao et al., 2010; Yang et al., 2012; Zhao et al., 2019; Zhang et al., 2020, 2021b). Thus, the Diaoyutai and Nanfen formations are constrained between ~ 1050 Ma and ~ 950 Ma. This is consistent with regional stratigraphic correlation: the Nanfen Formation has been correlated with the Xinxing Formation in the Xuzhou area of Jiangsu Province and the Liulaobei Formation in the Huainan region of Anhui Province (Su, 2016; Zhao et al., 2019; Zhang et al., 2021c), both of which have been estimated to be *ca.* 1086 Ma in depositional age (Zhang et al., 2022).

3. Previous palaeontological study of the Diaoyutai Formation

Paleontology work on the Diaoyutai Formation was mainly carried out in the late 1980 s and early 1990 s (e.g., Yin, 1980, 1983; Lin, 1984; Hong, 1989; Hong et al., 1991). Abundant carbonaceous compressions, including *Chuaria* and *Tawuia*, have been reported from the Diaoyutai Formation in the Fuxian District, Dalian City (Lin, 1984). The macrofossil assemblage is dominated by *Chuaria* (~80%) and *Tawuia* (~10–20%). These carbonaceous compressions were often interpreted

as macroalgae (e.g., Teyssèdre, 2003; Qian et al., 2008; Tang et al., 2017; Li et al., 2019). If correct, they represent a taxonomic diversification and ecological rise of eukaryotes at the Meso-Neoproterozoic transition.

Organic-walled microfossils from the Diaoyutai Formation, however, have not studied thoroughly. Yin (1980, 1983) conducted the first and only investigation of Diaoyutai OWMs collected from core ZK67 drilled in Anshan City, eastern Liaoning Province, and described 24 species belonging to 16 genera, but many of these specimens were not properly identified nor adequately illustrated (see Supplementary Data Table S1). Yin's (1983) results suggest a relatively simple assemblage of OWMs dominated by sphaeromorphs and their aggregates, characterized by thin-walled vesicles with compression folds but few ornamentations. The diameter of the vesicles ranges from ~ 40 to ~ 70 μm (Yin, 1983). Since the taxonomy of OWMs has evolved since the 1980 s and some taxonomic criteria used in the past have been shown to be taphonomic artifacts (e.g., Tang et al., 2013; Miao et al., 2021), it is necessary to reevaluate the systematic paleontology of the Diaoyutai OWMs.

4. Materials and methods

4.1. Acquisition of OWMs

In this study, twenty samples of dark grey shale and silty shale were collected from the Diaoyutai Formation at the Miaoshan section. Samples DYT–1 to DYT–4 were collected from the lower Diaoyutai Formation (Fig. 2c), and samples DYT–5 to DYT–20 from the middle-upper part of this formation (Fig. 2e). The procedure applied for palynological analysis was modified from Tang et al. (2013) and Miao et al. (2019). First, samples (rock chips with the size of ~ 0.2 cm^3, 60 g of each sample) were processed, using low-manipulation hydrofluoric (HF) acid maceration techniques, in the Geobiology laboratory of the School of Earth Sciences, China University of Geosciences, Wuhan (CUG–Wuhan). Acid residues were rinsed with DI-water to pH neutral state and then sieved gently through a nylon mesh (mesh size 15 μm) to remove small kerogen particles. No centrifuging and chemical oxidation treatments were applied.

Individual microfossil specimens were initially observed under a stereomicroscope, then transferred to clean glass slides using a micropipette and permanent strew mounts were made using cedar resin. The prepared slides were examined under a transmitted-light microscope (TLM) (ZEISS Axioscope 5) in the Geobiology laboratory of CUG–Wuhan. Microfossils were photographed on a digital camera (Axiocam 506 color CCD) attached to the TLM with the aid of software "ZEN core v3.0". Photomicrographs were taken at different focal levels and combined using "ZEN core v3.0" software to create a "Z-stack" composite image to visualize each microfossil fully. Measurement of microfossils was conducted on photomicrographs using the software "Digimizer Version 4.6.1". All illustrated specimens are deposited in the geobiology laboratory of CUG–Wuhan.

4.2. Micro-Raman spectroscopic analysis

A total of 398 Raman spectra were collected from 22 fossil specimens recovered from sample DYT–17. In order to assess the impact of palynological procedures on Raman characteristics, 36 Raman spectra of organic particles were collected *in situ* from three thin sections of sample DYT–17, –18, and –20. Raman spectra were obtained on a WITec alpha 300R confocal Raman imaging system with a 532 nm green laser source and a Zeiss microscope at the State Key Laboratory of Biogeology and Environmental Geology, CUG–Wuhan. Raman spectroscopic data were acquired and processed using the software WITec Project Five. The laser beam diameter was focused to<2 μm in diameter with a 50 × objective lens (N.A. = 0.75) to collect inelastically scattered photons. The laser power at the sample was maintained at *ca.* 0.5–1.5 mW to minimize sample damage related to laser-induced heating. The number of Raman spectra acquired for each fossil specimen varied from 13 to 23. Each single-point Raman spectrum was acquired as the accumulations of 2–4 scans of 20 s.

The acquired Raman spectral range was set to be between 0 and 3200 cm^{-1}, but only the range of 1000–1800 cm^{-1} was used for baseline correction and deconvolution, in order to focus on the Raman signal of carbonaceous material. The procedures for data processing are described below. First, the background fluorescence is removed by performing a baseline correction of the raw Raman spectra. Second, the baseline-corrected spectra were then decomposed into four component bands (D1, D2, D3, and D4 bands) using the fitting scheme of Kouketsu et al. (2014) for low metamorphic grade carbonaceous material, as is appropriate for the Diaoyutai Formation studied here. The calculated Lorentz functions were then added as linear combinations to obtain modeled Raman spectra, which fit the base-line corrected Raman spectra with a coefficient (R^2) higher than 0.99. Third, after deconvolution, the full width at half maxima (FWHM) was extracted for each peak.

5. Results and discussion

5.1. Diversity of OWMs

In total, ~980 specimens of OWMs were recovered from the analyzed samples. All specimens are deposited at the Department of Geobiology, School of Earth Sciences, CUG-Wuhan, and the systematic paleontology of these fossils can be found in the supplementary materials.

Except for three samples (DYT–3, –4, and –9), all other samples were found to contain abundant fossils. Most specimens (~83%) were recovered from samples DYT–10 to –20, and samples DYT–17 to –20 account for ~ 47% of the abundance and 73% of the taxa. Overall, 14 species belonging to 9 genera, as well as several unnamed or unidentified forms are described on the basis of morphological features (Fig. 3). For the convenience of discussion, they are grouped into four morphological categories: simple acritarchs (SA; Figs. 4 and 5), complex acritarchs (CA; Fig. 6), unbranched filamentous microfossils (FM; Figs. 8 and 9), and branched filamentous microfossils (BM; Figs. 10 and 11). The stratigraphic distributions of each group fossil as well as its relative abundance are demonstrated in Fig. 12. The higher fossil abundance and diversity in the middle Diaoyutai Formation (DYT–14 to –20) might be ascribed to better preservation in mudstone compared with that in the silty mudstone of the lower and upper intervals. However, the specific factors require further investigation.

5.1.1. Simple acritarchs

Simple acritarchs have a simple vesicle without any conspicuous ornamentation on the vesicle wall. These are the predominant components of the Diaoyutai assemblage, including isolated spheroidal vesicles of *Leiosphaeridia* (Fig. 4), aggregated *Leiosphaeridia* vesicles (Fig. 5a, b), elongated vesicles of *Navifusa* (Fig. 5c), aggregated vesicles of *Synsphaeridium* (Fig. 5d–f), and an unnamed form A (Fig. 5g–l). Among these taxa, *Leiosphaeridia* is the most abundant (>95%) and is present in all fossiliferous samples. The vesicle size of *Leiosphaeridia* ranges from 51 to 716 μm with an average of 248 ± 105 μm (n = 490), except for one specimen reaching as large as 1383 μm.

According to the taxonomic scheme proposed by Jankauskas et al. (1989) and adopted by Butterfield et al. (1994) and Tang et al. (2013), three *Leiosphaeridia* species can be recognized in the Diaoyutai assemblage, including *L. crassa* (Fig. 4a), *L. tenuissima* (Fig. 4b, c), and *L. jacutica* (Fig. 4d–o). *Leiosphaeridia crassa* and *L. jacutica* are both characterized by a thick vesicle wall, with the former species having a smaller vesicle (<70 μm in diameter) and the latter having a larger vesicle ranging from 70 to 800 μm in diameter. *Leiosphaeridia tenuissima* is featured by a thin vesicle wall and an intermediate vesicle diameter (~70–200 μm). Among these species, *L. jacutica* is the most abundant species. Most *L. jacutica* vesicles have compressional folds (e.g., Fig. 4d,

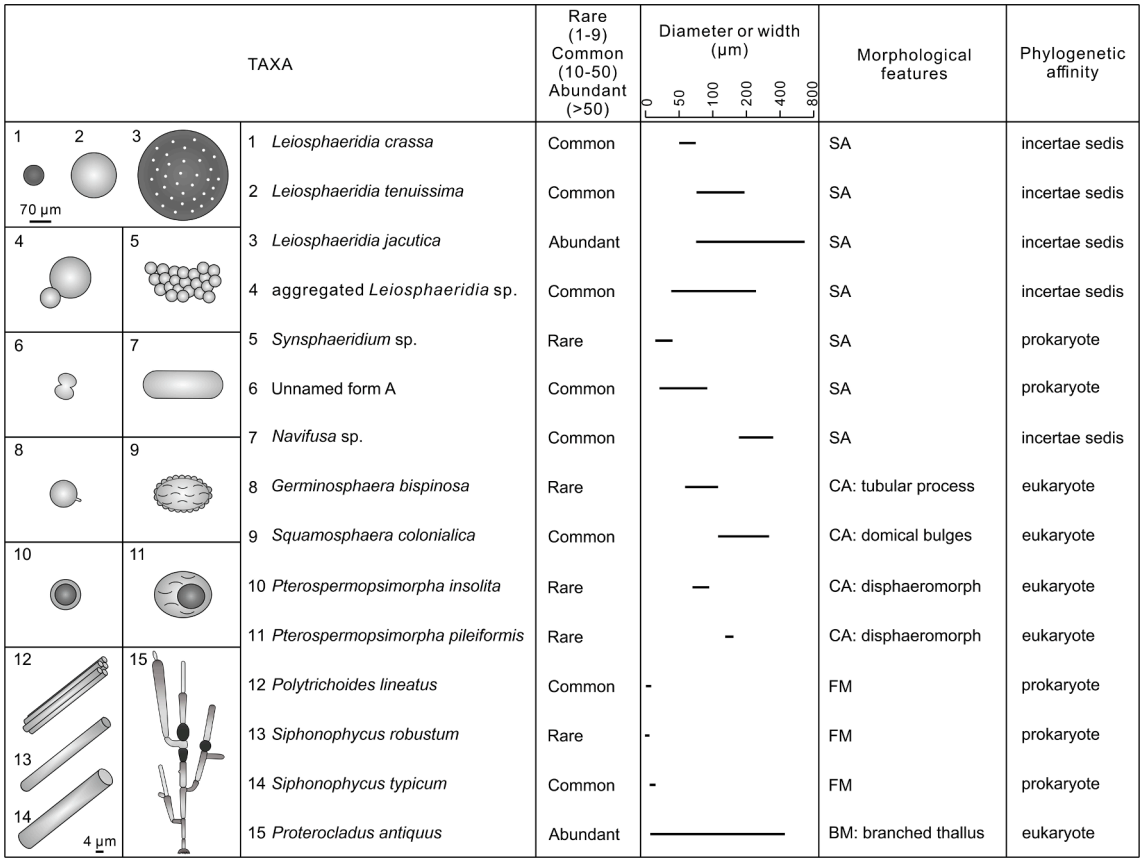

Fig. 3. List of taxa in the Diaoyutai fossil assemblages, including information about relative abundance, fossil size, morphological features, and probably phylogenetic affinity. Scale bars in schematic drawings are approximate. For morphological features, SA: simple acritarch; CA: complex acritarch; FM: unbranched filamentous microfossil; BM: branched microfossil.

k, m), and as a result show uneven translucency. Some *L. jacutica* vesicles bear an aperture-like structure (Fig. 4f) and possible medial split, probably representing taphonomic ruptures. Notably, several *L. jacutica* specimens show an enormous size (>600 μm in diameter; Fig. 4n, o). Some *Leiosphaeridia* vesicles, which would be identified as *L. crassa* if preserved individually, form aggregates of two or three vesicles (Fig. 5a, b). These aggregates are tentatively identified as *Leiosphaeridia* sp. In addition, *Navifusa* sp. (Fig. 5c) is a netromorphic form with an elongated, smooth-walled vesicle, the aspect ratios (i.e., the ratio between the maximum and minimum diameters) vary from 1.6 to 2.9, which is larger than that of *Leiosphaeridia* vesicles (<1.5).

Other aggregates that involve a greater number of relatively smaller vesicles are assigned to the genus *Synsphaeridium*, which is a rare occurrence in the Diaoyutai assemblage. Vesicles of *Synsphaeridium* sp. (Fig. 5d–f) are characterized by several to dozens of irregularly arranged spheroidal vesicles in aggregates, and the diameter of cells is around ~ 15–40 μm. Unnamed form A consists of dyad and tetrad arrangements without a common sheath (Fig. 5g–l); the dyads and tetrads likely resulted from cell division. The cells are 21–62 μm in width and 28–88 μm in length (n = 13). Several middle Proterozoic successions also have similar forms (Oehler, 1978; Jankauskas et al., 1989; Hermann, 1990; Miao et al., 2021), but their cells are smaller than the dyads and tetrads described here.

5.1.2. Complex acritarchs

The Diaoyutai assemblage contains approximately one hundred moderately to well-preserved OWMs with complex morphological features such as sculpture on vesicle wall, processes, internal body, and excystment structure. Three important genera are identified, including *Germinosphaera* (Fig. 6a–d), *Pterospermopsimorpha* (Fig. 6e, f), and *Squamosphaera* (Fig. 6g–i). Furthermore, one taxonomically unidentified specimen seems to have three poorly preserved processes (Fig. 6j), another has a vase-shaped morphology (Fig. 6k), and a third specimen has a vesicle with a granular texture and a distinct circular girdle (Fig. 6l).

Germinosphaera bispinosa exhibits a single unbranched process (or extension) that extends from vesicle walls (Butterfield et al., 1994). The vesicle diameter of specimens in the Diaoyutai assemblage ranges from 61 to 118 μm (average = 80, n = 9), and the processes are 9–22 μm in length (as measured on incompletely preserved processes, n = 9) and 5–11 μm in basal width (n = 9). The processes are hollow and openly connected with the vesicle cavity (Fig. 6d). The distal end of the processes is variable, and it can be tapering (Fig. 6a, c), rounded (Fig. 6b), or broken (Fig. 6d).

The genus *Pterospermopsimorpha* is a disphaeromorph with a spheroidal vesicle enclosing another smaller inner spheroidal vesicle, so the inner vesicle appears to have a greater optical opacity than the outer vesicle (Tang et al., 2013; Riedman and Porter, 2016). The thickness and texture of the outer vesicle can vary among species (Jankauskas et al., 1989; Hofmann and Jackson, 1994). One well-preserved specimen from the Diaoyutai assemblage is assigned to *P. insolita* due to its smooth outer wall (Fig. 6e). The diameters of the outer and inner vesicles of this specimen are around 68 μm and 52 μm, respectively. Thus, the ratio of the inner to outer vesicle diameter of *P. insolita* is 0.76. *Pterospermopsimorpha insolita* is different from *P. pileiformis* in its smoother vesicle wall and greater ratio of inner to outer vesicle diameter (Jankauskas et al., 1989). For example, *P. pileiformis* (Fig. 6f) in the Diaoyutai assemblage is ~ 75 μm in inner vesicle diameter, and ~ 172 μm in outer vesicle diameter, with an inner/outer vesicle diameter ratio of ~ 0.43.

About fourteen sub-spheroidal to spheroidal specimens, 107–321 μm

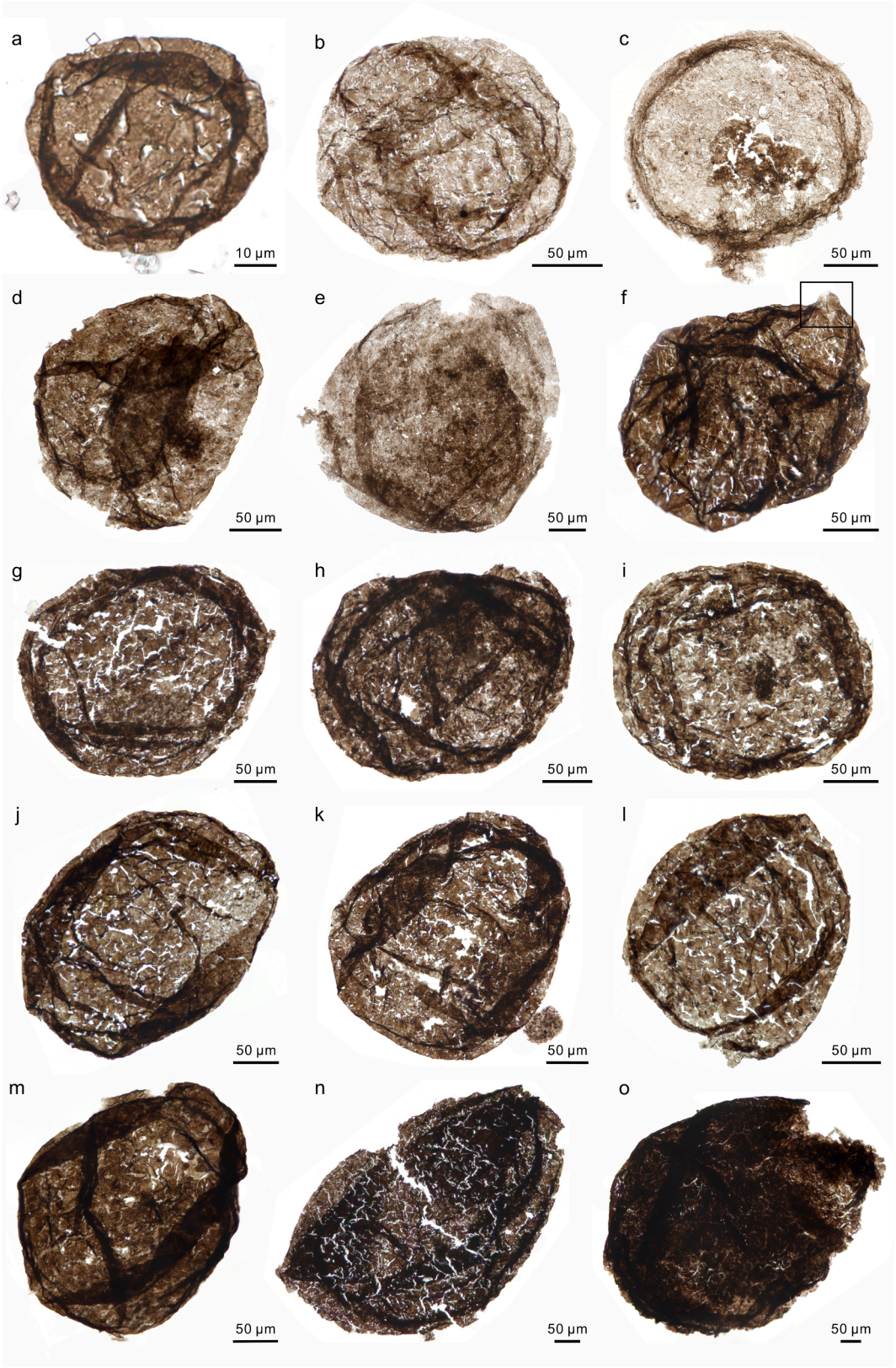

Fig. 4. Simple acritarchs. (a) *Leiosphaeridia crassa*. (b, c) *Leiosphaeridia tenuissima*. (d–o) *Leiosphaeridia jacutica*. Rectangle in (f) marks a small aperture or rupture. (a) DYT–15–002–84; (b) DYT–12–003–82; (c) DYT–6–002–86; (d) DYT–10–009–83; (e) DYT–12–005–83; (f) DYT–10–017–81; (g) DYT–13–001–86; (h) DYT–14–005–85; (i) DYT–14–001–88; (j) DYT–8–001–85; (k) DYT–16–010–83; (l) DYT–14–001–95; (m) DYT–11–001–84; (n) DYT–16–005–81; (o) DYT–12–004–81.

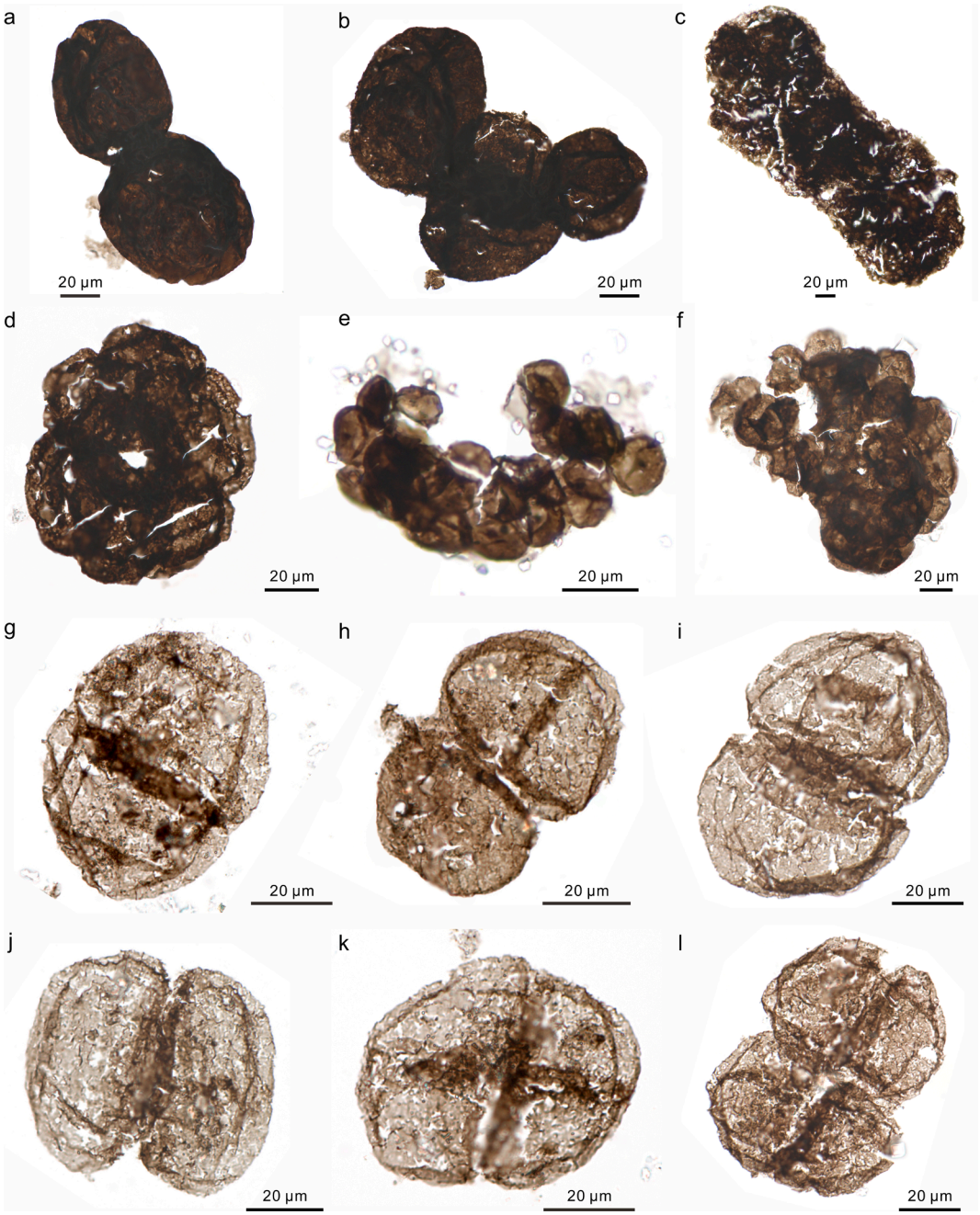

Fig. 5. Simple acritarchs. (a–b) Aggregated vesicles of *Leiosphaeridia* sp. (c) *Navifusa* sp. (d–f) *Synsphaeridium* sp. (g–l) Unnamed form A. (a) DYT–18–81; (b) DYT–19–002–89; (c) DYT–18–007–90; (d) DYT–15–015–83; (e) DYT–10–4; (f) DYT–10–9; (g) DYT–15–013–08; (h) DYT–15–014–81; (i) DYT–15–010–85; (j) DYT–15–001–82; (k) DYT–15–013–09; (l) DYT–15–005–86.

(n = 14) in dimension, are assigned to *Squamosphaera colonialica* (Fig. 6g–i) (Jankauskas, 1979; Tang et al., 2015). The vesicle of *S. colonialica* bears a moderate number of broadly domical bulges 10–50 μm (n = 14) in basal width.

5.1.3. Unbranched filamentous microfossils

About ninety unbranched filamentous microfossil specimens were recovered from the Diaoyutai Formation. These specimens are preserved as bundled or aggregated filaments (Figs. 8 and 9). Following previous taxonomic studies (e.g., Hofmann and Jackson, 1994), these fossils are best assigned to the genera *Polytrichoides* (Fig. 8) and *Siphonophycus* (Fig. 9).

Polytrichoides lineatus is characterized by tightly bundled, smooth-walled, unbranched, cylindrical filaments with one or two capitate ends (Fig. 8). Each filament may represent a cylindrical sheath of uniseriate microbes, but a common sheath surrounding the entire bundle is absent. Those bundles are 194–696 μm in length and 3.2–4.9 μm in width.

Siphonophycus specimens are preserved as isolated filaments or loosely to densely packed aggregates (Fig. 9). The filaments likely represent cylindrical sheaths of microbes, particularly filamentous cyanobacteria. Previous researchers have recognized eight morphological species of *Siphonophycus*, including *S. thulenema* (~0.5 μm in diameter), *S. septatum* (1–2 μm), *S. robustum* (2–4 μm), *S. typicum* (4–8 μm), *S. kestron* (8–16 μm), *S. solidum* (16–32 μm), *S. punctatum* (32–64 μm), and *S. gigas* (64–128 μm) (Maithy, 1975; Butterfield et al., 1994; Tang et al., 2013; Loron et al., 2019a). The Diaoyutai specimens have a diameter of 2–8 μm, and they can be classified as *S. typicum*

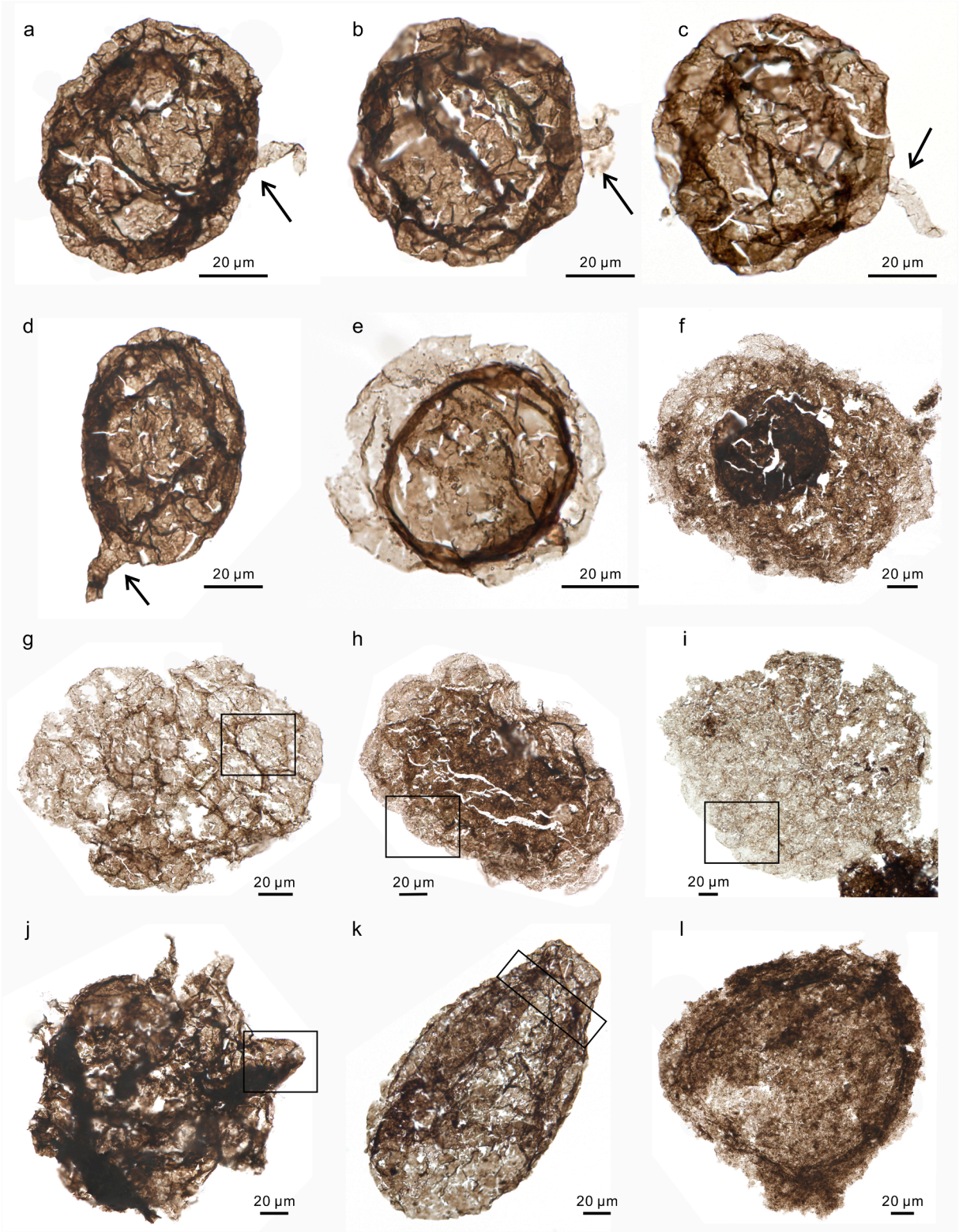

Fig. 6. Complex acritarchs. (a–d) *Germinosphaera bispinosa*. Arrows mark tail-like tubular process, which is hollow, often broken at terminal end, and communicates freely with vesicle cavity (d). (e) *Pterospermopsimorpha insolita*. (f) *Pterospermopsimorpha pileiformis*. (g–i) *Squamosphaera colonialica*. Rectangles denote domical bulges. (j–l) unidentified microfossils. Rectangle in (j) denotes papillate process, and rectangle in (k) marks neck-like constriction. (a) DYT–20–027–83; (b) DYT–20–029–84; (c) DYT–20–002–82; (d) DYT–14–008–85; (e) DYT–7–010–80; (f) DYT–14–006–83; (g) DYT–20–028–88; (h) DYT–15–010–81; (i) DYT–14–001–97; (j) DYT–18–005–88; (k) DYT–17–004–13; (l) DYT–17–015–85.

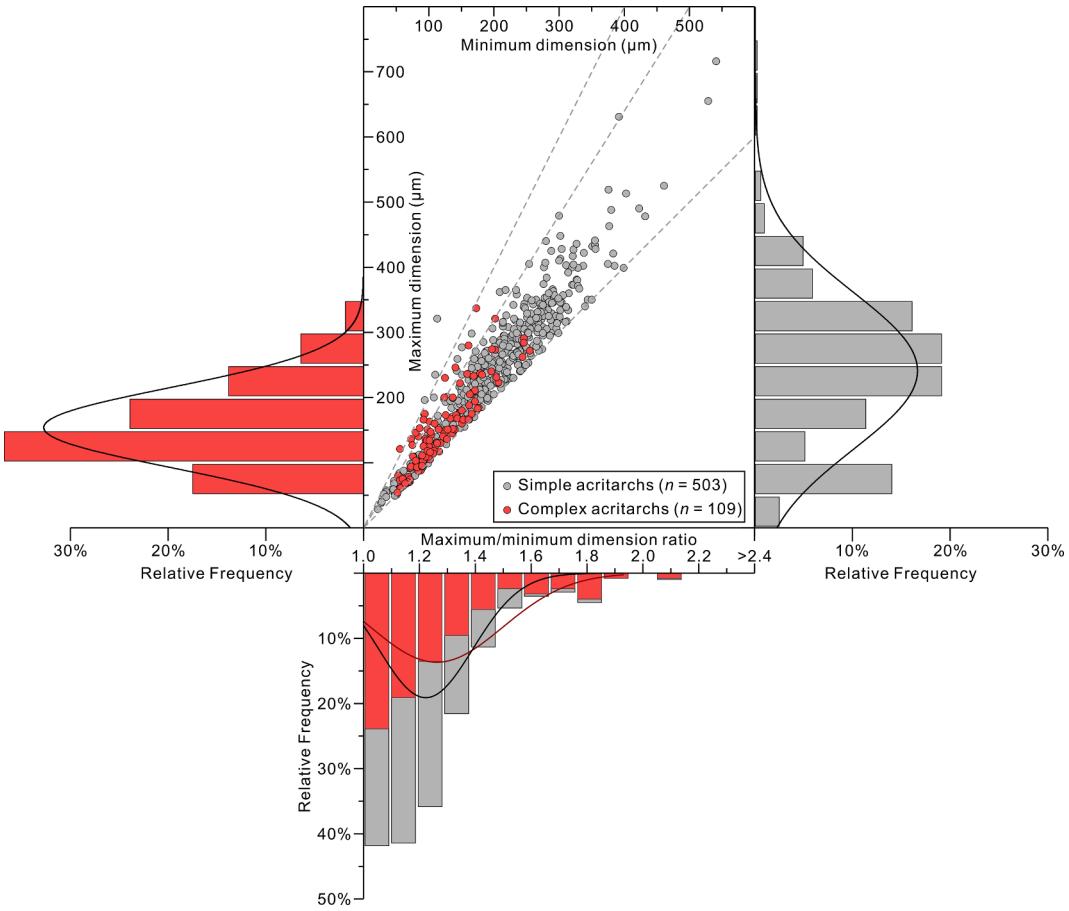

Fig. 7. Maximum and minimum dimensions, aspect ratio, and frequency distribution of simple (gray) and complex acritarchs (red, including unidentified microfossils). Frequency distribution histograms are fitted with kernel density curves.

(Fig. 9a–c, e, f) and *S. robustum* (Fig. 9d).

5.1.4. *Branched filamentous microfossils*

Relatively well-preserved branched filamentous microfossils are present in the Diaoyutai assemblage, mainly from samples DYT–17, –18, and –20, which yielded 239 specimens (Figs. 10 and 11). Most specimens are fragmented, due to taphonomic breakage or mechanical damage during fossil preparation. Generally, the fossils consist of uniseriate multicellular filaments that branch sparsely or profusely. Secondary branches are inserted laterally and asymmetrically, either unilaterally on one side of the parent filament (Fig. 10f) or alternately on both sides (Fig. 11l). Multiple orders of lateral branches can occur (Fig. 11p), leading to a complex thallus with numerous branches (Fig. 10c). A holdfast is possibly preserved in one of the specimens (Fig. 11d).

Cells within the filaments are delineated by septa or constrictions (Fig. 10a, d). Most cells are thin-walled and cylindrical or clavate in shape (Fig. 11l), and some are globose, cyathiform (Fig. 10d), and doliform in shape (Fig. 10f). A few opaque cells with a large width/length ratio are considered heteromorphic cells (Fig. 10d). In addition, some light-colored terminal cells have a distinctly narrow apical extension (Fig. 10a; Fig. 11g), possibly representing apical cell division. All lateral branches are initiated below a septum or constraint, and they either communicate with (Fig. 10b) or are separated from the main branch by a septum at the branching point (Fig. 11o). Largely opaque spherical bodies are present within some cells (red rectangles in Fig. 11d, k), and some hemispheroidal structures are developed, either individually or in clusters, on some filaments (Fig. 11k).

More completely preserved specimens reach a maximum length of ~ 1100 μm (Fig. 10a, c), indicating that complete thalli were millimeter-sized organisms. The diameter of the main axis and lateral branches ranges from 11 to 41 μm (average = 19.6 μm; $n = 153$; Fig. 13) and 10 to 24 μm (average = 16.6 μm, $n = 110$), respectively. Based on measurements on well-preserved cells, the cells are around 15–420 μm in length (average = 114 μm, $n = 72$) and 9–27 μm in width (average = 16 μm, $n = 72$), with a length/width ratio of 1.1–23.9 (average = 7.3, $n = 72$).

These morphological characteristics described above suggest that the branched filamentous microfossils are fragments of the green alga *Proterocladus*. The genus *Proterocladus* was first reported from the late Tonian Svanbergfjellet Formation in Svalbard by Butterfield et al. (1994), who differentiated three species, i.e., *P. minor* (3–7 μm in diameter), *P. hermannae* (7–14 μm in diameter), and *P. major* (10–35 μm in diameter). Subsequently, Tang et al. (2020) reported abundant well-preserved *Proterocladus* fossils from the Nanfen Formation at a site within 25 km from the section studied here, and described these fossils as *P. antiquus*. The species *P. major*, *P. minor*, and *P. hermannae* were distinguished by their cell size and the frequency of intercellular septa or constrictions (Butterfield et al., 1994). However, our materials show that cell width, septa, and constrictions can be variable even in the same specimen. Therefore, cell size alone may not be a reliable criterion for differentiating species of *Proterocladus*, particularly if they are preserved as fragments (Tang et al., 2020). Nonetheless, our specimens are morphologically similar to *P. antiquus* in the Nanfen assemblage (Tang et al., 2020) and they are tentatively identified as *P. antiquus*.

Fig. 8. Unbranched filamentous organic-walled microfossils. (a–g) *Polytrichoides lineatus* is characterized by tightly bundled, smooth-walled, unbranched filaments with one or two capitate ends. (a) DYT–11–002–83; (b) DYT–16–013–89; (c) DYT–20–004–86; (d) DYT–14–009–86; (e) DYT–20–028–93; (f) DYT–15–011–83; (g) DYT–15–004–81.

5.2. Comparison with other Meso-Neoproterozoic microfossil assemblages

The well-preserved OWMs assemblage in the Diaoyutai Formation records a relatively moderate morphological diversity, consisting of sphaeromorphs, acanthomorphs, unbranched filamentous aggregates, and branched filamentous microfossils. The Diaoyutai assemblage shares some taxonomic similarities with other Meso-Neoproterozoic microfossil assemblages (e.g., Tang et al., 2013; Baludikay et al., 2016; Beghin et al., 2017; Li et al., 2019; Loron et al., 2019a). Most of the spheroidal acritarchs (e.g., *Leiosphaeridia* and *Navifusa*), aggregated sphaeromorph vesicles (e.g., *Synsphaeridium*), and unbranched filamentous aggregates (e.g., *Polytrichoides* and *Siphonophycus*) have long stratigraphic and wide geographic ranges. For example, the bundled filamentous fossil *P. lineatus* is widely distributed in Proterozoic rocks, including northern America (Hofmann and Jackson, 1994; Loron et al., 2021), western and central Africa (Baludikay et al., 2016; Beghin et al., 2017), southeastern Siberia (Hermann, 1990), eastern European platform (Vorob'eva et al., 2015), and North China (Tang et al., 2013, 2015; Li et al., 2019). However, we note that simple leiospheres in the Diaoyutai assemblage are characterized by their large vesicles (500–700 μm in diameter, Fig. 7), generally larger than those reported in other Meso-Neoproterozoic assemblages; for example, leiospheres in the *ca.* 1350 Ma Xiamaling Formation have a maximum diameter of ~ 300 μm (Miao et al., 2021).

Fig. 9. Unbranched filamentous organic-walled microfossils. (a–c, e, f) *Siphonophycus typicum*, 4–8 μm in diameter; (d) *Siphonophycus robustum*, 2–4 μm in diameter. (a) DYT–19–001–91; (b) DYT–19–001–87; (c) DYT–19–001–82; (d) DYT–14–007–88; (e) DYT–17–004–20; (f) DYT–17–004–24.

We also note that the Diaoyutai assemblage has a lower taxonomic diversity, particularly in acanthomorphs, than microfossil assemblages from other Meso-Neoproterozoic units such as the Atar/El Mreïti Group in Mauritania, northwestern Africa (Beghin et al., 2017), Mbuji-Mayi Supergroup in Democratic Republic of Congo, central Africa (Baludikay et al., 2016), lower Shaler Supergroup in Arctic Canada (Loron et al., 2019a), and the Liulaobei and Tongjiazhuang formations in the Jiao-Liao-Xu-Huai regions of North China (Table S1). The Diaoyutai assemblage has thus far yielded only one acanthomorph species, *Germinosphaera bispinosa* (Fig. 6a–d), which is a widely distributed acanthomorph in Meso-Neoproterozoic sedimentary sequences (e.g., Butterfield et al., 1994; Baludikay et al., 2016; Loron and Moczydłowska, 2017; Miao et al., 2021; Loron et al., 2019a, 2021). In comparison, the lower Shaler Supergroup (*ca.* 1230 Ma to 900 Ma) contains a handful of acanthomorph species, including *Trachyhystrichosphaera aimika*, *Gigantosphaeridium fibratum*, *Herisphaera arbovela*, *H. triangula*, *Germinosphaera bispinosa,* and *Comasphaeridium tonium* (Loron et al., 2019a). Among these species, *T. aimika* has been commonly found in the late Mesoproterozoic Era to the Tonian Period, *ca.* 1150 Ma to 720 Ma (Baludikay et al., 2016; Pang et al., 2020a), and have been widely observed in the Jiao-Liao-Xu-Huai regions, e.g., the Liulaobei, Gouhou and Tongjiazhuang formations (Tang et al., 2013, 2015; Li et al., 2019). Another common Meso-Neoproterozoic OWM genus is *Simia*, which has been observed in the Liulaobei Formation (Tang et al., 2013), Atar/El Mreïti Group (Beghin et al., 2017), lower Shaler Supergroup (Loron et al., 2019a), and Xiamaling Formation (Miao et al., 2021), but enigmatically absent from the Diaoyutai assemblage (although the specimen illustrated in Fig. 6l may be a poorly preserved specimen of *Simia*). The absence or scarcity of *Trachyhystrichosphaera* and *Simia* from the Diaoyutai assemblage is intriguing and may be a result of inadequate sampling or inappropriate paleoenvironmental conditions.

What makes the Diaoyutai assemblage stand out is the abundant occurrence of *Proterocladus antiquus*, which was first described from the Nanfen Formation (1050–950 Ma) by Tang et al. (2020). The genus

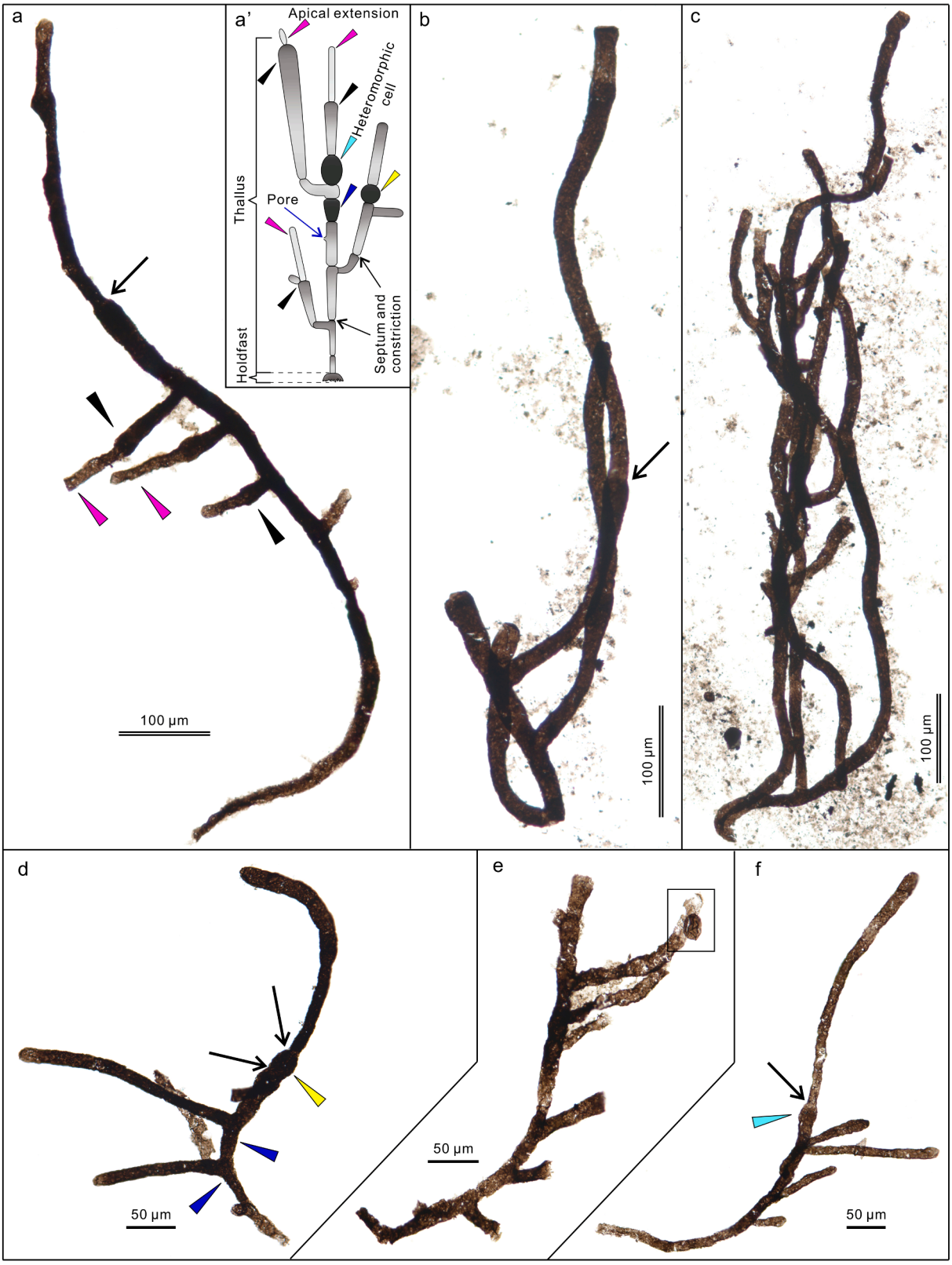

Fig. 10. *Proterocladus antiquus*. (a–f) Relatively complete specimens. (a') Morphological reconstruction and terminology, adapted from Tang et al. (2020). Black arrows denote complete septa or cell constrictions; black arrowheads, clavate cells; cyan arrowheads, doliform cells; blue arrowheads, cyathiform cells; yellow arrowheads, globose cells; purple arrowheads, apical extensions. (a) DYT–17–022–85; (b) DYT–17–025–082. (c) DYT–17–026–081; (d) DYT–17–005–84; (e) DYT–17–024–85; (f) DYT–17–024–83.

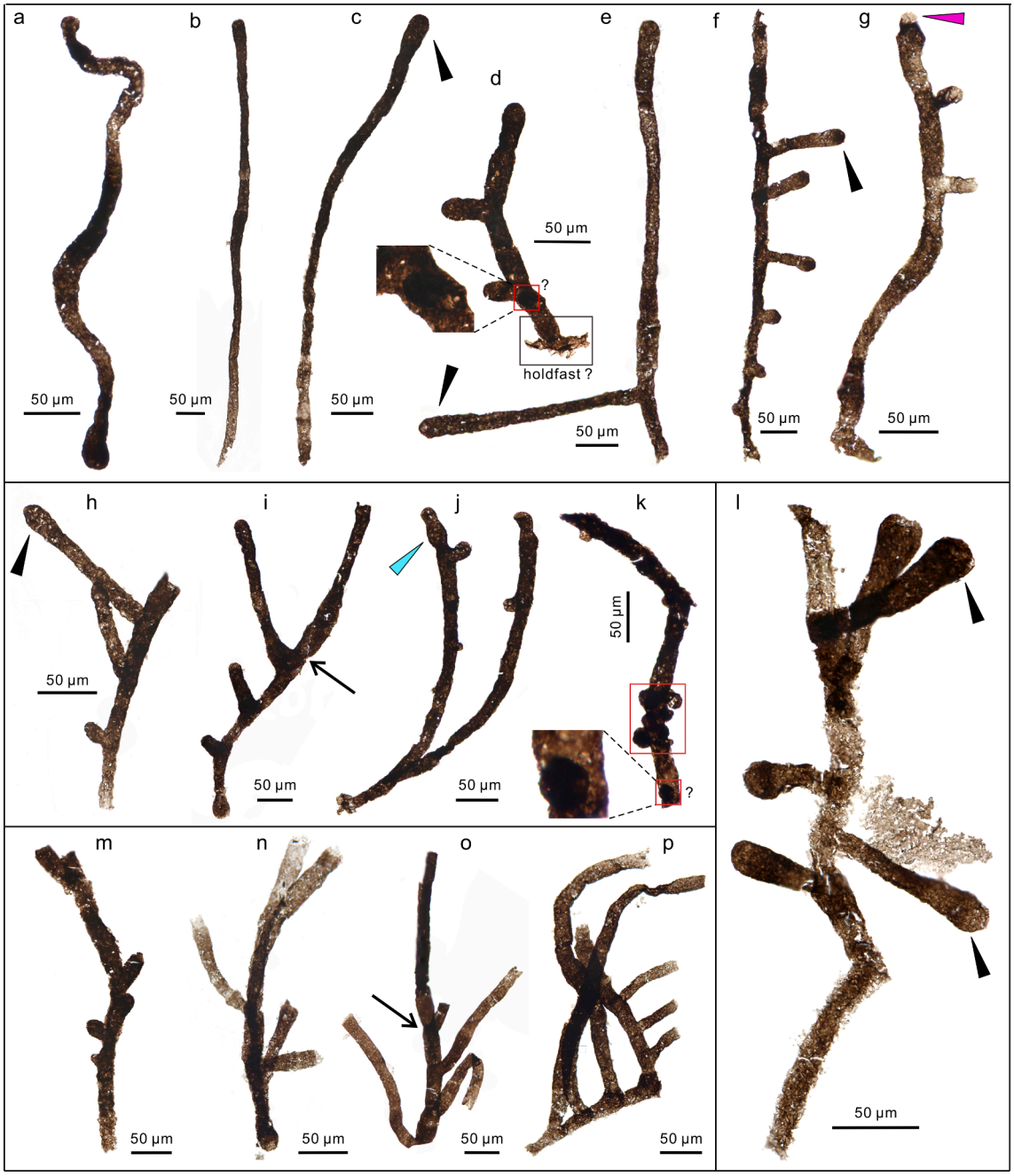

Fig. 11. Fragments of *P. antiquus*. Fragments with unbranched filaments (a–c), unilateral branches (d–k), alternate branches (l–o), and multiple orders of lateral branches (p). See Fig. 10 for arrow and arrowhead annotation. (a) DYT–20–015–83; (b) DYT–14–008–81; (c) DYT–17–012–85; (d) DYT–18–004–92; (e) DYT–17–021–82; (f) DYT–18–005–83; (g) DYT–19–004–84; (h) DYT–14–009–81; (i) DYT–16–013–91; (j) DYT–16–013–92; (k) DYT–20–011–85; (l) DYT–17–021–85; (m) DYT–20–001–82; (n) DYT–17–005–82; (o) DYT–17–024–84; (p) DYT–17–003–83.

Proterocladus has been observed in the Svanbergfjellet Formation (*ca.* 811.5–752.7 Ma) of Svalbard (Butterfield et al., 1994; Butterfield, 2015), and broadly similar forms also occur in the Khastakh Formation (*ca.* 820–720 Ma) of Siberia (Nagovitsin et al., 2015) and the Nonesuch Formation (*ca.* 1078 ± 24 Ma) in North America (Wellman and Strother, 2015; Strother and Wellman, 2021). Several clavate-shaped filaments from the Gouhou (Tang et al., 2015) and Liulaobei formations (unpublished), which are 1086–720 Ma in age (Wan et al., 2019; Pang et al., 2021; Zhang et al., 2022), may also be fragments of *Proterocladus*.

The Diaoyutai occurrence of *Proterocladus antiquus* is as old as, if not older than its occurrence in the Nanfen Formation (Tang et al., 2020), although both are constrained between 1050 Ma and 950 Ma (Fig. 1). According to the regional stratigraphy, the Diaoyutai Formation underlies the Nanfen Formation, which suggests that the fossils studied here are older than those reported in Tang et al. (2020). However, it has to be noted that these two reports are from different localities. At the Miaoshan section studied here, the base of the Nanfen Formation is defined by a glauconite-containing quartz sandstone, and the lower Nanfen Formation mainly consists of sandy carbonate (Qiao et al., 2001). However, the lower Nanfen Formation at the section studied by Tang et al. (2020) is characterized by dark grey and yellowish-green silty shale and mudstone where their *Proterocladus* fossils came from, and grayish argillaceous limestone occurs in the middle Nanfen Formation. Thus, direct stratigraphic correlation between these two fossil sites remains challenging because of possible facies variations, and it is possible that the *Proterocladus*-bearing strata in Tang et al. (2020) and

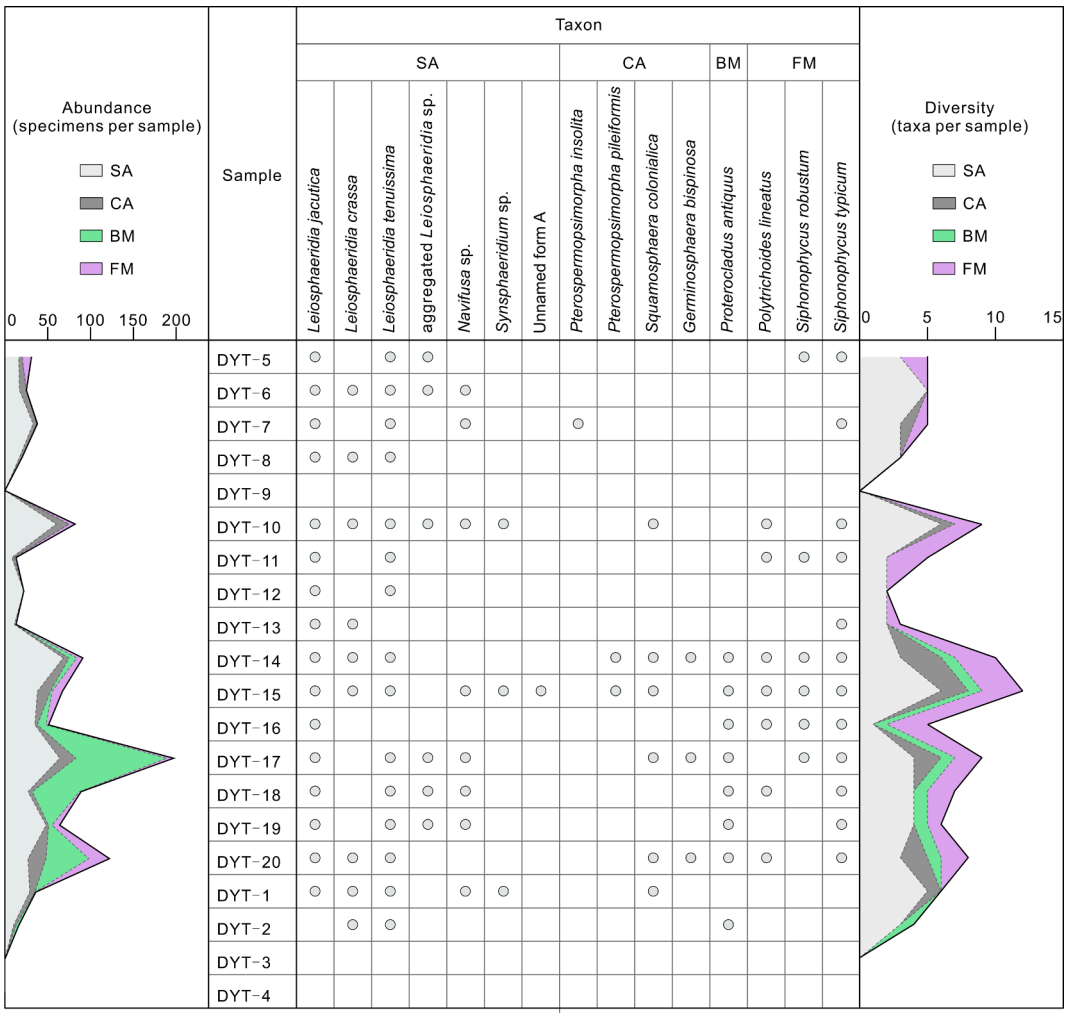

Fig. 12. Fossil occurrences, specimen abundance, and relative diversity of each Diaoyutai sample analyzed in this study. SA: simple acritarch; CA: complex acritarch; FM: unbranched filamentous microfossil; BM: branched microfossil.

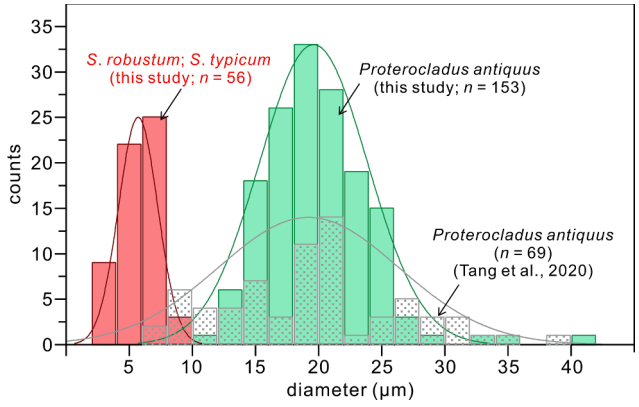

Fig. 13. Measured diameter of unbranched filamentous microfossils and branched specimens of *P. antiquus* from Tang et al. (2020) and this study. Frequency distribution histograms are fitted with kernel density curves.

this study are equivalent. Nonetheless, given that both the Diaoyutai and Nanfen formations are constrained between 1050 Ma and 950 Ma, it is safe to conclude that *P. antiquus* specimens from the Diaoyutai Formation are among the oldest known occurrences. The occurrence of *P. antiquus* adds more evidence indicating that the eukaryotic organisms were far more complex than previously imagined during the Meso-Neoproterozoic oceans.

5.3. Biological compositions of the Diaoyutai assemblage

The Diaoyutai assemblage contains a number of eukaryotic fossils, the most important of which is *Proterocladus antiquus*. On the basis of a suite of morphological characteristics, e.g., asymmetrical lateral branches, differentiated holdfast, akinete-like heteromorphic cells, swollen apical cell, and the absence of a common outer sheath, *P. antiquus* has been interpreted as a total-group siphonocladalean chlorophyte (Tang et al., 2020) or a total-group ulvophycean chlorophyte (Hou et al., 2022). The presence of holdfast in the *P. antiquus* (Fig. 11d, see also fig. 1 and Extended Data fig. 4 in Tang et al., 2020) Tang et al., 2020) suggests that it was a benthic alga standing above the seafloor for photosynthesis.

Other eukaryotic fossils in the Diaoyutai microfossil assemblage include *Germinosphaera bispinosa*, *Pterospermopsimorpha insolita*, and *P. pileiformis* according to their complex vesicle morphologies (e.g., Baludikay et al., 2016; Agić et al., 2017; Beghin et al., 2017; Loron and Moczydłowska, 2017). The tubular or cylindrical processes of *Germinosphaera* (Fig. 6a–d) are somewhat similar to those of the putative fungal fossil *Ourasphaira giraldae* recovered from shallow-water estuarine shale of the Grassy Bay Formation, Shaler Supergroup in Arctic Canada (Loron et al., 2019b). *Ourasphaira giraldae* is 33–80 μm in vesicle diameter, 10–35 μm in process length, bears a single process that is septate and branches repeatedly (Loron et al., 2019b; their fig. 1a–g). In contrast, *G. bispinosa* from the Diaoyutai assemblage bears a single

cylindrical, non-septate, and non-branching process. Nonetheless, *G. bispinosa* is likely a eukaryote and its phylogenetic relationship with *O. giraldae* merits further investigation. As disphaeromorphs, *Pterospermopsimorpha insolita* and *P. pileiformis* are generally considered to be eukaryotes (e.g., Baludikay et al., 2016; Agić et al., 2017; Beghin et al., 2017; Loron et al., 2019a; Miao et al., 2021). Recently, Li et al. (2019) pointed out that the inner vesicle may represent condensed cytoplasm, but the Diaoyutai specimens have a translucent inner vesicle, likely representing a hollow organic-walled structure rather than a solid structure of condensed cytoplasm (Fig. 6e). It is likely that these complex acritarchs were planktonic eukaryotes (Javaux and Knoll, 2016; Beghin et al., 2017).

Squamosphaera colonialica from the Diaoyutai assemblage is also a possible eukaryote. The domical bulges of *S. colonialica* could be impressions of cells that once existed within the vesicle interior, indicating a multicellular organism (Vidal and Ford, 1985; Tang et al., 2015). They are superficially similar to the polygonal plates in *Satka,* but their domical morphology is best discernable at the edge of the vesicle. *Squamosphaera colonialica* has been interpreted as a eukaryote (Vidal and Ford, 1985; Tang et al., 2015; Porter and Riedman, 2016), although Javaux and Knoll (2016) suggested that it may be a prokaryotic organism analogous to pleurocapsalean cyanobacteria. In the present study, we classify it as a possible eukaryote.

In addition to eukaryotic fossils, abundant prokaryotic fossils are also present in the Diaoyutai assemblage. These include aggregated and unbranched filamentous forms such as *Polytrichoides lineatus*, *Siphonophycus typicum,* and *S. robustum*, as well as aggregated spheroidal forms such as *Synsphaeridium* sp. Aggregated unbranched filaments such as *S. typicum* and *S. robustum* observed in this study are interpreted as fragments of microbial mats constructed by filamentous cyanobacteria (Butterfield et al., 1994; Tang et al., 2013). Thus, these specimens represent benthic microbes. In addition, specimens of *P. lineatus* with a common sheath have been revealed in the Tongjiazhuang Formation and many other coeval sequences [see summary in Li et al. (2019)]. Thus, the absence of an outer sheath in the Diaoyutai specimens of *P. lineatus* could be the result of taphonomic loss. Nonetheless, *P. lineatus* is here regarded as a cyanobacterium.

The phylogenetic interpretation of the genus *Leiosphaeridia* is controversial. The main differences among the three *Leiosphaeridia* species in the Diaoyutai assemblage, i.e., *L. crassa*, *L. tenuissima*, and *L. jacutica*, are the vesicle diameter and vesicle wall thickness (Butterfield et al., 1994). For these simple leiospheres, vesicle size can provide suggestive, but not definitive, evidence for prokaryote vs. eukaryote affinities. Generally, prokaryotic cells range from 0.1 to 5.0 μm in diameter and are notably smaller than eukaryotic cells, which are typically 10–100 μm in cell size. The difference in cell size is because eukaryotic cells have a large nucleus and a complex cytoskeleton system, which can sustain complex metabolism and provide support for large cells (Pang et al., 2015). As such, large spheroidal fossils (>300 μm in diameter) from the Mesoproterozoic have been suggested to be possible eukaryotes (Javaux and Lepot, 2018). *Leiosphaeridia* spp. in the Diaoyutai assemblage ranges from 51 to 716 μm in vesicle diameter, with an average of 248 ± 105 μm ($n = 490$), similar to or larger than the vesicle size of complex acritarchs in the assemblage, which ranges from 54 to 337 μm in vesicle diameter, with an average of 154 ± 61 μm ($n = 109$). Thus, large simple spheroidal acritarchs in the Diaoyutai assemblage, particularly those with a vesicle diameter > 300 μm, are regarded as possible eukaryotes, although we emphasize that this interpretation is by no means conclusive because cell sizes of eukaryotic and prokaryotic cells do overlap (Javaux et al., 2003; Javaux and Lepot, 2018). In addition, these large specimens may represent the collective envelope of a much smaller colonial microbe. However, the current specimens display a homogeneous inner structure, which cannot tell whether it represents an intact cell or is caused by preservation. Future work is required to test this. Considering that *Leiosphaeridia* are cosmopolitan elements, it is likely that this group of organisms were planktonic.

In summary, the Diaoyutai assemblage reveals that eukaryotes and prokaryotes are both present in shallow marine environments at the Mesoproterozoic-Neoproterozoic transition (Fig. 15). In these environments, benthic microbial mats constructed by filamentous cyanobacteria thrived on the seafloor within the photic zone, millimeter-sized benthic green algae such as *P. antiquus* stood above the sediment–water interface, and planktonic prokaryotic and eukaryotic organisms colonized the water column. According to the recovered Diaoyutai fossil assemblage, the relative abundance of eukaryotic fossils is relatively high (Fig. 14). Convincing eukaryotic fossils account for 27.2%, including *Proterocladus antiquus* (24.4%), *Squamosphaera colonialica* (1.4%), *Germinosphaera bispinosa* (0.8%), and *Pterospermopsimorpha* spp. (0.6%). If *Leiosphaeridia* specimens with a diameter of > 300 μm are counted toward eukaryotes, the abundance of eukaryotes reaches as high as 42.8%. We note that the relative abundance of *Proterocladus antiquus* may be overestimated because most specimens are fragments. Furthermore, it has to be pointed out that these estimations may not represent the natural marine ecosystem compositions as all spherical specimens smaller than 15 μm (due to the method used) and most of the spherical specimens with the size between 15 and 30 μm (the limitation of manually picking) were lost during sample processing. Most of these lost specimens might be prokaryotes. Nevertheless, this ecosystem reconstruction implies that the water column was oxic, at least at ecological time scales.

The relative abundance of eukaryotes, a critical parameter of an ecosystem, of the Precambrian shallow marine ecosystem is a fascinating topic but remains controversial. From the perspective of body fossil, such as the study carried here, multiple types of eukaryotes have been recovered, including some complex specimens, e.g., *Proterocladus antiquus* (e.g., Javaux et al., 2001; Beghin et al., 2017; Miao et al., 2021; Eckford-Soper et al., 2022; this study). Although we cannot discount the possibility that eukaryotic organisms may have had a greater preservation potential than prokaryotes, and most of the prokaryotic specimens were lost during the sample processing, eukaryotic contribution to sedimentary organic carbon in the Diaoyutai assemblage is not negligible. In contrast, the lack of eukaryote biomarkers in sediments older than 820 Ma suggests that the fraction of eukaryotes, if present, was limited (below the instrumental detection limit) (e.g., Luo et al., 2015, 2016; Brocks et al., 2017; Gueneli et al., 2018; Zumberge et al., 2019). The absence of steranes in this time period has also been ascribed to the preservation bias related to the mat-seal effect, which would have formed a significant mechanical and biochemical barrier to in-falling plankton (Pawlowska et al., 2013). Therefore, the inconsistency between the body fossil and biomarker records calls for further investigations to solve the potential bias in both aspects.

5.4. Burial thermal history of the Diaoyutai assemblage

The representative Raman spectra of three OWMs and carbonaceous material in thin sections are shown in Fig. 16, and the complete data are provided in Supplementary Data Table S2. All raw Raman spectra show two broad peaks, the D band (~1350 cm^{-1}) and G band (1600 cm^{-1}), and the intensity of the decomposed D2 band is greater than that of the D1 band (Fig. 16), indicating relatively low-grade thermal maturity perhaps < 300 ℃ (e.g., Beyssac et al., 2002; Rahl et al., 2005; Lahfid et al., 2010; Buseck and Beyssac, 2014; Kouketsu et al., 2014; Henry et al., 2019). The relatively low estimated metamorphic temperature is supported by a resolvable D4-band (Fig. 16) on the shoulder of the D1-band, which suggests that the peak metamorphic temperature is lower than ~ 250 ℃ (Lahfid et al., 2010).

Considering the relatively low metamorphic temperature in our initial assessment as discussed above, the specific burial temperature (T-D1) of the Diaoyutai assemblage can be further quantified using the Raman parameter FWHM-D1 according to the calibrated geothermometer of Kouketsu et al. (2014), T-D1 (℃) = − 2.15 × (FWHM–D1) + 478 (calibration error ± 30 ℃). Since the formula

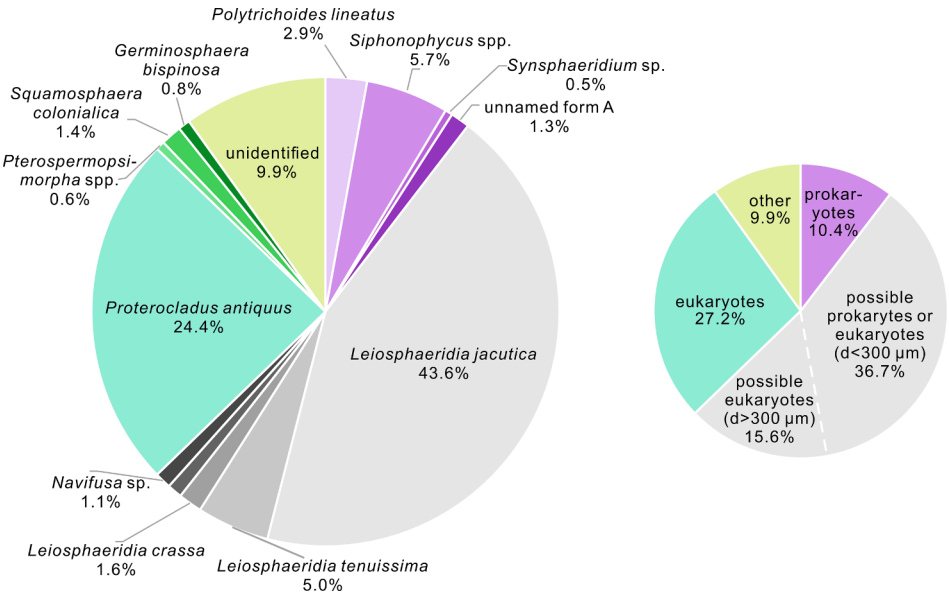

Fig. 14. Relative species abundance and proportions of different microfossil groups from the Diaoyutai Formation. In the pie diagram to the right, taxa are grouped according to their most likely phylogenetic interpretations, with the hues of wedges matching those in the pie diagram to the left.

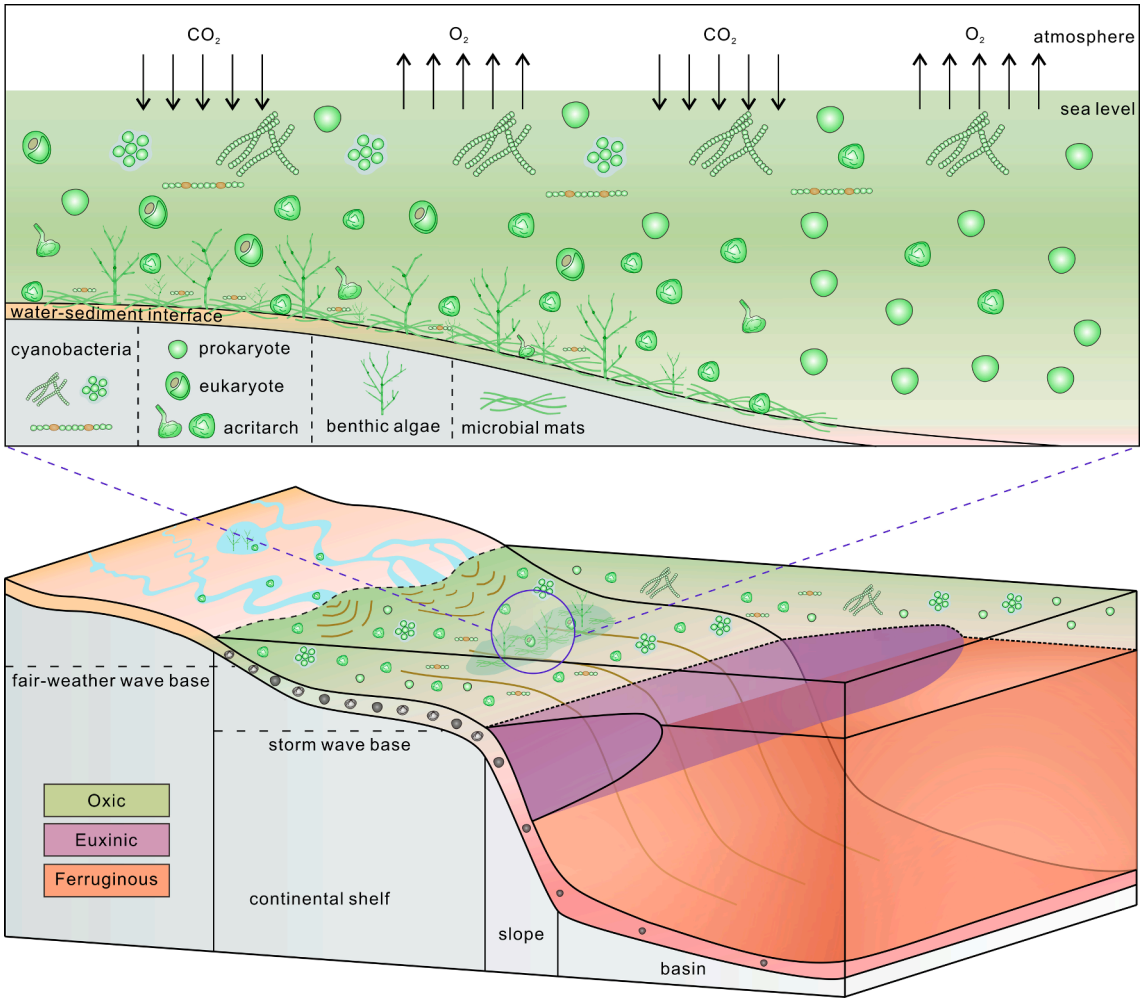

Fig. 15. Reconstruction of marine redox conditions (lower) and coastal marine ecosystem (upper) in Meso-Neoproterozoic coastal oceans. The marine redox model is modified from Canfield (1998) and Li et al. (2010).

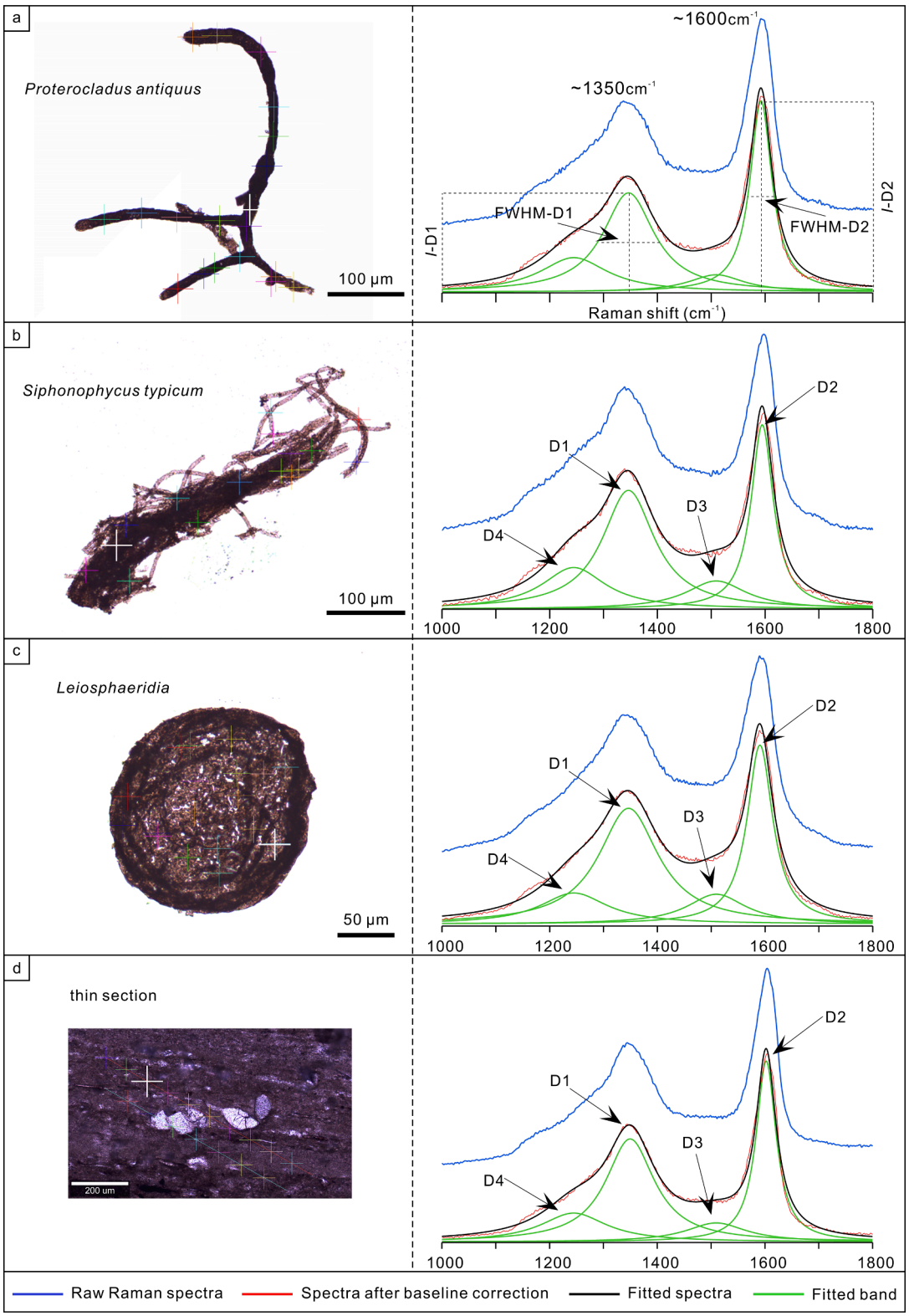

Fig. 16. Representative Raman spectra of organic-walled microfossils (a, *Proterocladus antiquus*; b, *Siphonophycus typicum*; c, *Leiosphaeridia* spp.) and carbonaceous material in thin sections (d) from the Diaoyutai Formation, illustrating the protocols of baseline correction, spectrum deconvolution, and spectral parameters. The crosses in a–d represent the positions of Raman analytical spots, with the white cross in each panel corresponding to the spectrum shown to the right.

calibrated by Kouketsu et al. (2014) is applicable in the range of 150–400 ℃, only the FWHM-D1 values within the range of 100–152 cm^{-1} can be applied to burial temperature calculation. For all Raman measurements (n = 434) of the Diaoyutai Formation, >96% of data is located in this range (see Table S2), supporting the application of the calibration of Kouketsu et al. (2014).

Following Kouketsu et al. (2014), the estimated burial temperatures based on the extracted OWMs and *in situ* carbonaceous materials are shown in Fig. 17. Two distinct characteristics are observed. First, each of the three extracted fossil groups (Fig. 17a – c) gives a wide range of T-

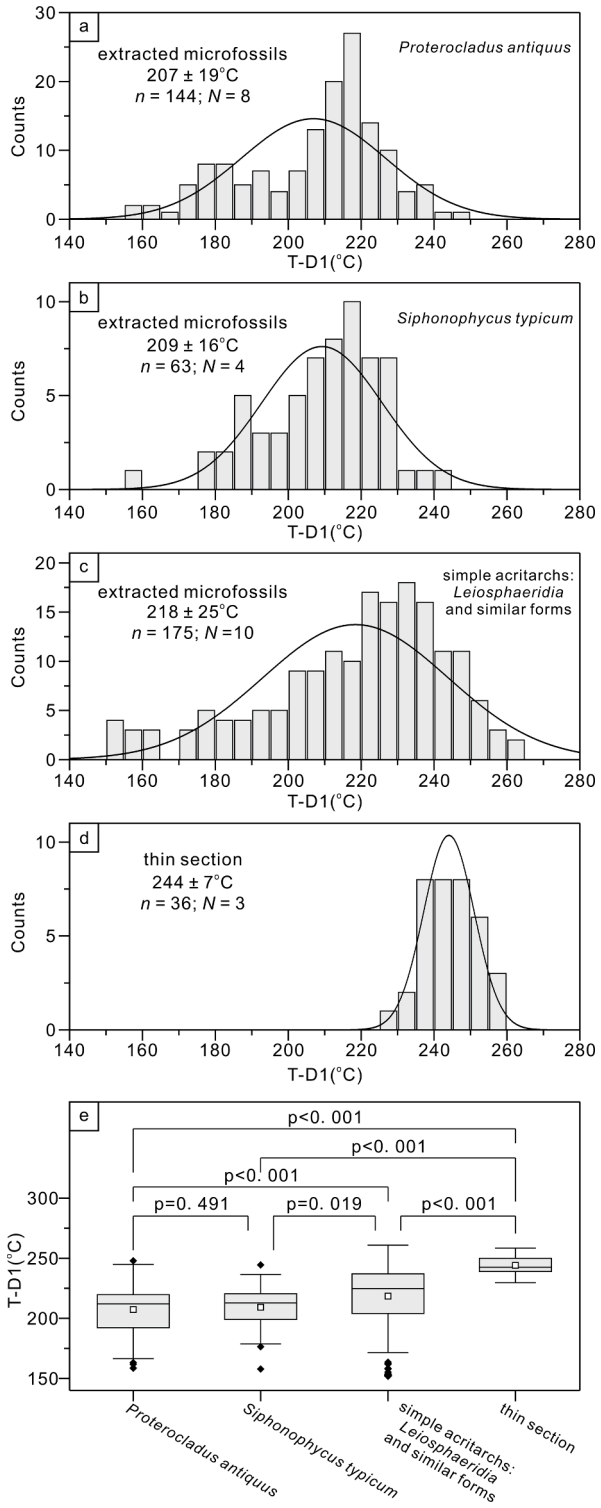

Fig. 17. Estimated T-D1 peak metamorphic temperatures of the Diaoyutai Formation based on carbonaceous material Raman geothermometric data collected from *in-situ* analysis of extracted microfossils of *P. antiquus* (a), extracted microfossils of *S. typicum* (b), extracted microfossils of simple acritarchs (*Leiosphaeridia* and similar forms, c), and carbonaceous material in thin sections (d). Box-and-whisker plots of the four morphogroups and paired comparison test results are shown in (e), where $p < 0.001$ denotes significant difference in T-D1. T-D1 peak metamorphic temperatures were calculated following Kouketsu et al. (2014). *N*, number of specimens or thin section analyzed; *n*, number of Raman spectra collected. Frequency distribution histograms are fitted with kernel density curves.

D1 temperatures, with a variance greater than the calibration error (± 30 ℃) of this method and the variance of T-D1 temperatures estimated from *in situ* carbonaceous materials (Fig. 17d). We are uncertain about the factors that led to the large variations observed in Raman spectroscopy of organic-walled microfossils in the Diaoyutai assemblage. We speculate that the differences in chemical compositions among different taxa or different structures of the same specimen, related to differences in precursor biomolecules or in secondary microbial degradation, might be the main factor. It has been suggested that subtle difference in precursor biomolecules may be registered in Raman spectroscopy of carbonaceous fossils (Qu et al., 2015, 2019; Pang et al., 2020b), and that microbial degradation can substantially affect the Raman spectrum characteristics of organic materials (Cañadas et al., 2022).

Second, the mean estimated burial temperatures from the extracted organic-walled microfossils and those from *in situ* carbonaceous materials are different (Fig. 17e). Specifically, the mean T-D1 temperatures estimated from *Proterocladus antiquus*, *Siphonophycus typicum*, and *Leiosphaeridia* plus similar forms are 207 ± 19 ℃ ($n = 144$), 209 ± 16 ℃ ($n = 63$), and 218 ± 25 ℃ ($n = 175$), respectively. However, the mean T-D1 temperatures from *in situ* carbonaceous material is 244 ± 7 ℃ ($n = 36$), significantly higher than those from the extracted organic-walled microfossils ($p < 0.001$; Fig. 17e). The difference observed here contrasts previous studies, which showed no significant difference in Raman geothermometric temperatures estimated from *in situ* carbonaceous material and extracted organic-walled microfossils (Baludikay et al., 2018), indicating that fossil extraction using hydrofluoric acid should not affect Raman spectroscopic results.

The Raman spectroscopic differences between extracted fossils and *in situ* carbonaceous material may be related to their chemical differences. Because the *in situ* analysis did not targeted on organic-walled microfossils, it is possible that detrital organic carbon was included in the analysis. For example, detrital graphite particles have been documented in sedimentary rocks, e.g., the late Mesoproterozoic Shennongjia Group in South China (Li et al., 2022), Cryogenian Nantuo Formation in South China (Ye et al., 2020) and Cenozoic marine sediment (Sparkes et al., 2020). However, if both detrital and indigenous organic carbon were included in the *in situ* Raman analysis, a greater variance would be expected because of the heterogeneous sources of carbonaceous material, contrary to the lower variance as observed in the T-D1 temperatures from *in situ* Raman analysis (Fig. 17d). Thus, we speculate that both extracted organic-walled microfossils and *in situ* carbonaceous material are indigenous to the Diaoyutai Formation, but their slightly different Raman spectroscopic signals may be related to different precursor biomolecules derived from different group of organisms. Considering that T-D1 temperatures from extracted fossils and *in situ* carbonaceous material largely overlap (Fig. 17), we decided to pool the data and estimated a peak metamorphic temperature of approximately 215 ± 23 ℃ ($n = 418$) for the Diaoyutai Formation.

The carbonaceous material Raman geothermometric data of the Diaoyutai Formation are broadly consistent with the burial history of Meso-Neoproterozoic sediments in the Jiao-Liao-Xu-Huai region of North China (Pang et al., 2020b). For example, the estimated T-D1 peak temperature of the Liulaobei Formation, which is widely distributed in the Huainan region, northern Anhui Province, North China, is ~ 201 ℃ based on Raman analysis of 44 microfossil specimens (Pang et al., 2020b). A metamorphic temperature of ~ 200 ℃ is also consistent with the excellent preservation of Meso-Neoproterozoic OWMs in the Jiao-Liao-Xu-Huai region. The Diaoyutai Formation and its stratigraphic equivalents (e.g., the Liulaobei Formation in Huainan of Anhui Province, and Shiwangzhuang and Tongjiazhuang formations in eastern Shandong Province) contain abundant well-preserved OWMs (e.g., Yin and Sun, 1994; Tang et al., 2013; Li et al., 2019, 2020; Han et al., 2020). These OWMs show similar colors ranging from medium yellow-orange to medium-dark brown, suggesting a thermal alteration index of 2 to 5, corresponding to a burial temperature around 200 ℃ (e.g., Staplin, 1969; Batten, 1996; Baludikay et al., 2018).

6. Conclusions

Well-preserved organic-walled microfossils are described in the *ca.* 1000 million-year-old Diaoyutai Formation in Dalian, Liaoning Province. A total of 14 species belonging to 9 genera, as well as several unnamed or unidentified forms are described, including simple and complex spherical acritarchs, unbranched filamentous microfossils, and branched forms. Raman spectral geothermometery of organic-walled microfossils shows that the Diaoyutai Formation experienced a peak metamorphic temperature of ~ 215 ℃, consistent with the burial history of Meso-Neoproterozoic sediments in the Jiao-Liao-Xu-Huai region and the colors of the OWMs in these sediments.

Diaoyutai OWMs are tentatively interpreted as unambiguous eukaryotes (*Germinosphaera bispinosa*, *Pterospermopsimorpha insolita*, *Pterospermopsimorpha pileiformis*, *Squamosphaera colonialica*, and *Proterocladus antiquus*), possible prokaryotes (*Polytrichoides lineatus*, *Siphonophycus robustum*, *Siphonophycus typicum*, *Synsphaeridium* sp., and Unnamed form A), and incertae sedis (*Leiosphaeridia crassa*, *L. tenuissima*, *L. jacutica*, *Navifusa* sp., and aggregated *Leiosphaeridia* sp.). Importantly, the green algal fossil *Proterocladus antiquus* is abundant in the Diaoyutai Formation, representing one of the earliest known occurrences of this taxon and providing a key constraint on the phylogenetic divergence of viridiplantae. The Diaoyutai assemblage helps us to develop a better understanding of the Meso-Neoproterozoic coastal marine ecosystem, where microbial mats consisting of filamentous cyanobacteria colonized the benthic realm, millimeter-sized benthic green algae rose from sediment surface and elevated into the water column, and micrometer-sized prokaryotic and eukaryotic organisms occupied the planktonic realm. The abundance of *Proterocladus* in the Diaoyutai assemblage indicates the ecological rise of photosynthetic eukaryotes and the modernization of the marine ecosytems in terms of major primary producers may have occurred earlier than previously thought.

Declaration of Competing Interest

The authors declare that they have no known competing financial interests or personal relationships that could have appeared to influence the work reported in this paper.

Data availability

share data

Acknowledgments

This study was supported by the National Natural Science Foundation of China (41821001, 42272001) and the Strategic Priority Research Program (B) of the Chinese Academy of Sciences (XDB26020102). Q. T. acknowledges additional supports from the National Key Research and Development Program of China (2022YFF0800303) and the Fundamental Research Funds for the Central Universities (0206-14380137). S. X. acknowledges support from the U.S. National Science Foundation (EAR-2021207). We thank Prof. Nick Butterfield and an anonymous reviewer for their constructive comments, which significantly improve the quality of this manuscript. Zhuoling Liu, Yalan Yuan, Chang Wang, Chenxi Wu, and Xingyu Ma are thanked for field assistance, and Dr. Daoliang Chu, Min Shi, and Qin Ye are acknowledged for laboratory assistance.

Appendix A. Supplementary material

Supplementary data to this article can be found online at https://doi.org/10.1016/j.precamres.2023.107104.

References

Adam, Z.R., Skidmore, M.L., Mogk, D.W., Butterfield, N.J., 2017. A Laurentian record of the earliest fossil eukaryotes. Geology 45, 387–390.
Agić, H., Małgorzata, M., Yin, L., 2015. Affinity, life cycle, and intracellular complexity of organic-walled microfossils from the Mesoproterozoic of Shanxi. China. J. Paleontol. 89, 28–50.
Agić, H., Moczydłowska, M., Yin, L., 2017. Diversity of organic-walled microfossils from the early Mesoproterozoic Ruyang Group, North China Craton-A window into the early eukaryote evolution. Precambrian Res. 297, 101–130.
Baludikay, B.K., Storme, J.Y., Francois, C., Baudet, D., Javaux, E.J., 2016. A diverse and exquisitely preserved organic-walled microfossil assemblage from the Meso-Neoproterozoic Mbuji-Mayi Supergroup (Democratic Republic of Congo) and implications for Proterozoic biostratigraphy. Precambrian Res. 281, 166–184.
Baludikay, B.K., François, C., Sforna, M.C., Beghin, J., Cornet, Y., Storme, J.Y., Fagel, N., Fontaine, F., Littke, R., Baudet, D., Delvaux, D., Javaux, E.J., 2018. Raman microspectroscopy, bitumen reflectance and illite crystallinity scale: comparison of different geothermometry methods on fossiliferous Proterozoic sedimentary basins (DR Congo, Mauritania and Australia). Int. J. Coal Geol. 191, 80–94.
Batten, D., 1996. Palynofacies and petroleum potential. Palynology: principles and applications 3, 1065–1084.
Beghin, J., Storme, J.-Y., Blanpied, C., Gueneli, N., Brocks, J.J., Poulton, S.W., Javaux, E. J., 2017. Microfossils from the late Mesoproterozoic–early Neoproterozoic Atar/El Mreïti Group, Taoudeni Basin, Mauritania, northwestern Africa. Precambrian Res. 291, 63–82.
Bengtson, S., Sallstedt, T., Belivanova, V., Whitehouse, M., 2017. Three-dimensional preservation of cellular and subcellular structures suggests 1.6 billion-year-old crown-group red algae. PLOS Biol. 15, e2000735 https://doi.org/10.1371/journal.pbio.2000735.
Betts, H.C., Puttick, M.N., Clark, J.W., Williams, T.A., Donoghue, P.C., Pisani, D., 2018. Integrated genomic and fossil evidence illuminates life's early evolution and eukaryote origin. Nat. Ecol. Evol. 2, 1556–1562.
Beyssac, O., Goffé, B., Chopin, C., Rouzaud, J.N., 2002. Raman spectra of carbonaceous material in metasediments: a new geothermometer. J. Metamorphic. Geol. 20, 859–871.
Blumenberg, M., Thiel, V., Riegel, W., Kah, L.C., Reitner, J., 2012. Biomarkers of black shales formed by microbial mats, Late Mesoproterozoic (1.1 Ga) Taoudeni Basin. Mauritania. Precambrian Res. 196–197, 113–127.
Brocks, J.J., Jarrett, A.J.M., Sirantoine, E., Hallmann, C., Hoshino, Y., Liyanage, T., 2017. The rise of algae in Cryogenian oceans and the emergence of animals. Nature 548, 578–581.
Buseck, P.R., Beyssac, O., 2014. From Organic Matter to Graphite: Graphitization. Elements 10, 421–426.
Butterfield, N.J., 2000. *Bangiomorpha pubescens* n. gen., n. sp.: implications for the evolution of sex, multicellularity, and the Mesoproterozoic/Neoproterozoic radiation of eukaryotes. Paleobiology 26, 386–404.
Butterfield, N.J., 2015. Early evolution of the Eukaryota. Palaeontology 58, 5–17.
Butterfield, N.J., Knoll, A.H., Swett, K., 1994. Paleobiology of the Neoproterozoic Svanbergfjellet Formation, Spitsbergen. Lethaia 27, 76–76.
Cañadas, F., Papineau, D., Leng, M.J., Li, C., 2022. Extensive primary production promoted the recovery of the Ediacaran Shuram excursion. Nat. Commun. 13, 148.
Canfield, D.E., 1998. A new model for Proterozoic ocean chemistry. Nature 396, 450–453.
Cohen, P.A., Kodner, R.B., 2021. The earliest history of eukaryotic life: uncovering an evolutionary story through the integration of biological and geological data. Trends Ecol. Evol. 37, 246–256.
Du, R., Wang, Q., Tian, L., 1995. Catalogue of algal megafossils from the Proterozoic of China. Precambrian Res. 73, 291–298.
Eckford-Soper, L.K., Andersen, K.H., Hansen, T.F., Canfield, D.E., 2022. A case for an active eukaryotic marine biosphere during the Proterozoic era. Proc. Natl. Acad. Sci. 119 e2122042119.
Evanovich, E., Guerreiro, J.F., 2020. A timescale for the radiation of photosynthetic eukaryotes. bioRxiv, doi.org/10.1101/2020.04.18.047969.
Fedonkin, M.A., Yochelson, E.L., 2002. Middle Proterozoic (1.5 Ga) *Horodyskia moniliformis* Yochelson and Fedonkin, the oldest known tissue-grade colonial Eucaryote. Smithson. Contrib. Paleobiol. 94, 29.
Gao, L., Zhang, C., Chen, S., Liu, P., Ding, X., Liu, Y., Dong, C., Song, B., 2010. Detrital zircon SHRIMP U-Pb age from the Diaoyutai Formation, Xihe Group in Liaodong Peninsula, China and its geological significance. Geol. Bull. China 29, 1113–1122.
Gibson, T.M., Shih, P.M., Cumming, V.M., Fischer, W.W., Crockford, P.W., Hodgskiss, M. S., Wörndle, S., Creaser, R.A., Rainbird, R.H., Skulski, T.M., 2017. Precise age of *Bangiomorpha pubescens* dates the origin of eukaryotic photosynthesis. Geology 46, 135–138.
Grey, K., Williams, I.R., 1990. Problematic bedding-plane markings from the Middle Proterozoic manganese subgroup, Bangemall Basin. Western Australia. Precambrian Res. 46, 307–327.
Grey, K., Yochelson, E.L., Fedonkin, M.A., Martin, D.M., 2010. *Horodyskia williamsii* new species, a Mesoproterozoic macrofossil from Western Australia. Precambrian Res. 180, 1–17.
Gueneli, N., McKenna, A.M., Ohkouchi, N., Boreham, C.J., Beghin, J., Javaux, E.J., Brocks, J.J., 2018. 1.1-billion-year-old porphyrins establish a marine ecosystem dominated by bacterial primary producers. Proc. Natl. Acad. Sci. 115. E6978–E6986.
Han, C., Chen, L., Li, G., Pang, K., Wang, W., Zhou, G., Yang, L., Lyu, W., Wang, K., Zhong, Z., Wu, C., Yang, F., 2020. First record of organic-walled microfossils from the Tonian Shiwangzhuang Formation of the Tumen Group in western Shandong, North China. Palaeoworld 30, 208–219.

Han, T.M., Runnegar, B., 1992. Megascopic eukaryotic algae from the 2.1-billion-year-old Negaunee Iron-Formation. Michigan. Science 257, 232–235.
Henry, D.G., Jarvis, I., Gillmore, G., Stephenson, M., 2019. Raman spectroscopy as a tool to determine the thermal maturity of organic matter: Application to sedimentary, metamorphic and structural geology. Earth-Sci Rev. 198, 102936 https://doi.org/10.1016/j.earscirev.2019.102936.
Hermann, T.N., 1990. Organic World Billion Year Ago. Academy of Sciences of the USSR, Instute of Precambrian Geology and Geochronology, Leningrad 1–48 [in Russian].
Hofmann, H.J., 1985. The mid-Proterozoic Little Dal macrobiota, Mackenzie Mountains, north-west Canada. Palaeontology 28, 331–354.
Hofmann, H.J., Jackson, G.D., 1994. Shale-facies microfossils from the Proterozoic Bylot Supergroup, Baffin Island. Canada. J. Paleontol. 68, 1–35.
Hong, Z., 1989. Development of research on Precambrian geology with their significance in southern Liaoning province. Liaoning Geology 87–94 [in Chinese].
Hong, Z., Yang, Y., Huang, F., 1991. Macrofossil sequence of the late Precambrian from the southern Liaodong peninsula. Liaoning Geology 219–236 [in Chinese].
Hou, Z., Ma, X., Shi, X., Li, X., Yang, L., Xiao, S., De Clerck, O., Leliaert, F., Zhong, B., 2022. Phylotranscriptomic insights into a Mesoproterozoic-Neoproterozoic origin and early radiation of green seaweeds (Ulvophyceae). Nat. Commun. 13, 1610. https://doi.org/10.1038/s41467-022-29282-9.
Jankauskas, T.V., Mikhailova, N.S., Hermann, T.N., 1989. Mikrofossilii dokembriya SSSR (Precambrian microfossils of the USSR): Leningrad, Trudy Instituta Geologii i Geochronologii Dokembria SSSR Akademii Nauk. Nauka 1–190 [In Russian].
Jankauskas, T.V., 1979. Srednerifeyski microbiota Yuzhnogo Urala i Bashkirskogo Priural'ya [Middle Riphean microbiota of the southern Urals and the Ural region in Bashkiria]: Akademii Nauk SSSR. Doklady (Proceedings of the USSR Academy of Sciences) 248, 190–193 [in Russian].
Javaux, E.J., Knoll, A.H., Walter, M., 2003. Recognizing and interpreting the fossils of early eukaryotes. Orig. Life Evol. Biosph. 33, 75–94.
Javaux, E.J., Knoll, A.H., 2016. Micropaleontology of the lower Mesoproterozoic Roper Group, Australia, and implications for early eukaryotic evolution. J. Paleontol. 91, 199–229.
Javaux, E.J., Knoll, A.H., Walter, M.R., 2001. Morphological and ecological complexity in early eukaryotic ecosystems. Nature 412, 66–69.
Javaux, E.J., Lepot, K., 2018. The Paleoproterozoic fossil record: Implications for the evolution of the biosphere during Earth's middle-age. Earth-Sci Rev. 176, 68–86.
Javaux, E.J., Marshal, C.P., 2006. A new approach in deciphering early protist paleobiology and evolution: Combined microscopy and microchemistry of single Proterozoic acritarchs. Rev. Palaeobot. Palynol. 139, 1–15.
Knoll, A.H., 2014. Paleobiological perspectives on early eukaryotic evolution. Cold Spring Harb. Perspect. Biol. 6, a016121 https://doi.org/10.1101/cshperspect.a016121.
Kouketsu, Y., Mizukami, T., Mori, H., Endo, S., Aoya, M., Hara, H., Nakamura, D., Wallis, S., 2014. A new approach to develop the Raman carbonaceous material geothermometer for low-grade metamorphism using peak width. Isl. Arc 23, 33–50.
Kumar, 2001. Mesoproterozoic megafossil *Chuaria–Tawuia* association may represent parts of a multicellular plant, Vindhyan Supergroup, Central India. Precambrian Res. 106, 187–211.
Lahfid, A., Beyssac, O., Deville, E., Negro, F., Chopin, C., Goffé, B., 2010. Evolution of the Raman spectrum of carbonaceous material in low-grade metasediments of the Glarus Alps (Switzerland). Terra nova 22, 354–360.
Lamb, D.M., Awramik, S.M., Chapman, D.J., Zhu, S., 2009. Evidence for eukaryotic diversification in the ~1800 million-year-old Changzhougou Formation. North China. Precambrian Res. 173, 93–104.
Lbgmr, 1989. Regional Geology of Liaoning Province. Geological Publishing House, Beijing.
Li, G., Chen, L., Pang, K., Zhou, G., Han, C., Yang, L., Lv, W., Wu, C., Wang, W., Yang, F., 2020. An assemblage of macroscopic and diversified carbonaceous compression fossils from the Tonian Shiwangzhuang Formation in western Shandong. North China. Precambrian Res. 346, 105801 https://doi.org/10.1016/j.precamres.2020.105801.
Li, C., Love, G.D., Lyons, T.W., Fike, D.A., Sessions, A.L., Chu, X., 2010. A stratified redox model for the Ediacaran ocean. Science 328, 80–83.
Li, D., Luo, G., Yang, H., She, Z., Papineau, D., Li, C., 2022. Characteristics of the carbon cycle in late Mesoproterozoic: Evidence from carbon isotope composition of paired carbonate and organic matter of the Shennongjia Group in South China. Precambrian Res. 377, 106726 https://doi.org/10.1016/j.precamres.2022.106726.
Li, G., Pang, K., Chen, L., Zhou, G., Han, C., Yang, L., Wang, W., Yang, F., Yin, L., 2019. Organic-walled microfossils from the Tonian Tongjiazhuang Formation of the Tumen Group in western Shandong, North China Craton and their biostratigraphic significance. Gondwana Res. 76, 260–289.
Lin, W., 1984. A preliminary study on carbonaceous macrofossils from late Precambrian strata in southern Liaodong Peninsula. Bulletin of Shenyang Institute of Geology and Mineral Resources, Chinese Academy of Geological Sciences 10, 131–152 [in Chinese].
Loron, C.C., Francois, C., Rainbird, R.H., Turner, E.C., Borensztajn, S., Javaux, E.J., 2019b. Early fungi from the Proterozoic era in Arctic Canada. Nature 570, 232–235.
Loron, C.C., Halverson, G.P., Rainbird, R.H., Skulski, T., Turner, E.C., Javaux, E.J., 2021. Shale-hosted biota from the Dismal Lakes Group in Arctic Canada supports an early Mesoproterozoic diversification of eukaryotes. J. Paleontol. 95, 1113–1137.
Loron, C.C., Moczydłowska, M., 2017. Tonian (Neoproterozoic) eukaryotic and prokaryotic organic-walled microfossils from the upper Visingsö Group, Sweden. Palynology 42, 220–254.
Loron, C.C., Rainbird, R.H., Turner, E.C., Greenman, J.W., Javaux, E.J., 2019a. Organic-walled microfossils from the late Mesoproterozoic to early Neoproterozoic lower Shaler Supergroup (Arctic Canada): Diversity and biostratigraphic significance. Precambrian Res. 321, 349–374.
Luo, Q., George, S.C., Xu, Y., Zhong, N., 2016. Organic geochemical characteristics of the Mesoproterozoic Hongshuizhuang Formation from northern China: Implications for thermal maturity and biological sources. Org. Geochem. 99, 23–37.
Luo, G., Hallmann, C., Xie, S., Ruan, X., Summons, R.E., 2015. Comparative microbial diversity and redox environments of black shale and stromatolite facies in the Mesoproterozoic Xiamaling Formation. Geochim. Cosmochim. Acta 151, 150–167.
Lyu, D., Deng, Y., Wang, X., Ye, Y., Pang, K., Miao, L., Luo, Z., Zhang, F., Lu, Y., Deng, S., Wang, H., Zhang, S., 2022. New chronological and paleontological evidence for Paleoproterozoic eukaryote distribution and stratigraphic correlation between the Yanliao and Xiong'er basins. North China Craton. Precambrian Res. 371, 106577.
Maithy, P., 1975. Microorganisms from the Bushimay System (Late Precambrian) of Kanshi, Zaire. The Paleobotanist 22, 133–149.
Miao, L., Moczydłowska, M., Zhu, S., Zhu, M., 2019. New record of organic-walled, morphologically distinct microfossils from the late Paleoproterozoic Changcheng Group in the Yanshan Range. North China. Precambrian Res. 321, 172–198.
Miao, L., Moczydłowska, M., Zhu, M., 2021. A diverse organic-walled microfossil assemblage from the Mesoproterozoic Xiamaling Formation. North China. Precambrian Res. 360, 106235 https://doi.org/10.1016/j.precamres.2021.106235.
Nagovitsin, K.E., Stanevich, A.M., Kornilova, T.A., 2010. Stratigraphic setting and age of the complex Tappania-bearing Proterozoic fossil biota of Siberia. Russ. Geol. Geophys. 51, 1192–1198.
Nagovitsin, K.E., Rogov, V.I., Marusin, V.V., Karlova, G.A., Kolesnikov, A.V., Bykova, N. V., Grazhdankin, D.V., 2015. Revised Neoproterozoic and Terreneuvian stratigraphy of the Lena-Anabar Basin and north-western slope of the Olenek Uplift. Siberian Platform. Precambrian Res. 270, 226–245.
Nguyen, K., Love, G.D., Zumberge, J.A., Kelly, A.E., Owens, J.D., Rohrssen, M.K., Bates, S.M., Cai, C., Lyons, T.W., 2019. Absence of biomarker evidence for early eukaryotic life from the Mesoproterozoic Roper Group: Searching across a marine redox gradient in mid-Proterozoic habitability. Geobiology 17, 247–260.
Oehler, D.Z., 1978. Microflora of the middle proterozoic balbirini dolomite (McArthur group) of Australia. Alcheringa 2, 269–309.
Pang, K., Tang, Q., Yuan, X.L., Wan, B., Xiao, S.H., 2015. A biomechanical analysis of the early eukaryotic fossil *Valeria* and new occurrence of organic-walled microfossils from the Paleo-Mesoproterozoic Ruyang Group. Palaeoworld 24, 251–262.
Pang, K., Tang, Q., Wan, B., Yuan, X., 2020a. New insights on the palaeobiology and biostratigraphy of the acritarch *Trachyhystrichosphaera aimika*: A potential late Mesoproterozoic to Tonian index fossil. Palaeoworld 29, 476–489.
Pang, K., Tang, Q., Wu, C., Li, G., Chen, L., Wan, B., Yuan, X., Bodnar, R.J., Xiao, S., 2020b. Raman spectroscopy and structural heterogeneity of carbonaceous material in Proterozoic organic-walled microfossils in the North China Craton. Precambrian Res. 346, 105818 https://doi.org/10.1016/j.precamres.2020.105818.
Pang, K., Tang, Q., Wan, B., Li, G.J., Chen, L., Yuan, X., Zhou, C., 2021. Integrated Meso-Neoproterozoic stratigraphy in the Jiao-Liao-Xu-Huai area of North China Craton: A review. Journal of Stratigraphy 45, 467–492. https://doi.org/10.19839/j.cnki.dcxzz.2021.0019.
Parfrey, L.W., Lahr, D.J., Knoll, A.H., Katz, L.A., 2011. Estimating the timing of early eukaryotic diversification with multigene molecular clocks. Proc. Natl. Acad. Sci. 108, 13624–13629.
Pawlowska, M.M., Butterfield, N.J., Brocks, J.J., 2013. Lipid taphonomy in the Proterozoic and the effect of microbial mats on biomarker preservation. Geology 41, 103–106.
Peng, Y., Bao, H., Yuan, X., 2009. New morphological observations for Paleoproterozoic acritarchs from the Chuanlinggou Formation. North China. Precambrian Res. 168, 223–232.
Porter, S.M., 2020. Insights into eukaryogenesis from the fossil record. Interface Focus 10, 20190105. https://doi.org/10.6084/m9.figshare. c.4948722.
Porter, S.M., Riedman, L.A., 2016. Systematics of organic-walled microfossils from the *ca.* 780–740 Ma Chuar Group, Grand Canyon. Arizona. J. Paleontol. 90, 815–853.
Porter, S.M., Agic, H., Riedman, L.A., 2018. Anoxic ecosystems and early eukaryotes. Emerg. Top. Life Sci. 2, 299–309.
Qian, M., Wang, Y., Yan, Y., 2008. Neoproterozoic biota on the southeastern margin of the North China paleocontinent. The Geological Publishing House 1–131 [in Chinese].
Qiao, X., Gao, L., Peng, Y., 2001. Neoproterozoic in the Tan-Lu fault belt: Cataclysm, sequence and Biology. The Geological Publishing House 1–141 [in Chinese].
Qu, Y., Engdahl, A., Zhu, S., Vajda, V., McLoughlin, N., 2015. Ultrastructural Heterogeneity of Carbonaceous Material in Ancient Cherts: Investigating Biosignature Origin and Preservation. Astrobiology 15, 825–842.
Qu, Y., McLoughlin, N., van Zuilen, M.A., Whitehouse, M., Engdahl, A., Vajda, V., 2019. Evidence for molecular structural variations in the cytoarchitectures of a Jurassic plant. Geology 47, 325–329.
Rahl, J.M., Anderson, K.M., Brandon, M.T., Fassoulas, C., 2005. Raman spectroscopic carbonaceous material thermometry of low-grade metamorphic rocks: Calibration and application to tectonic exhumation in Crete. Greece. Earth Planet Sci Lett. 240, 339–354.
Riedman, L.A., Porter, S., 2016. Organic-walled microfossils of the mid-Neoproterozoic Alinya Formation, Officer Basin. Australia. J. Paleontol. 90, 854–887.
Sergeev, V.N., Vorob'eva, N.G., Petrov, Y.u., P.,, 2017. The biostratigraphic conundrum of Siberia: Do true Tonian-Cryogenian microfossils occur in Mesoproterozoic rocks? Precambrian Res. 299, 282–302.
Sforna, M.C., Loron, C.C., Demoulin, C.F., Francois, C., Cornet, Y., Lara, Y.J., Grolimund, D., Ferreira Sanchez, D., Medjoubi, K., Somogyi, A., Addad, A., Fadel, A., Compere, P., Baudet, D., Brocks, J.J., Javaux, E.J., 2022. Intracellular bound

chlorophyll residues identify 1 Gyr-old fossils as eukaryotic algae. Nat. Commun. 13, 146. https://doi.org/10.1038/s41467-021-27810-7.
Sharma, M., Singh, V.K., 2019. Megascopic Carbonaceous Remains from Proterozoic Basins of India, Geological Evolution of the Precambrian Indian Shield. Springer 725–749.
Shi, M., Feng, Q., Khan, M., Awramik, S., Zhu, S., 2017. Silicified microbiota from the Paleoproterozoic Dahongyu Formation, Tianjin. China. J. Paleontol. 91, 369–392.
Sparkes, R.B., Hovius, N., Galy, A., Liu, J.T., 2020. Survival of graphitized petrogenic organic carbon through multiple erosional cycles. Earth Planet Sci Lett. 531, 115992 https://doi.org/10.1016/j.epsl.2019.115992.
Staplin, F.L., 1969. Sedimentary organic matter, organic metamorphism, and oil and gas occurrence. Bull. Can. Pet. Geol. 17, 47–66.
Strassert, J.F.H., Irisarri, I., Williams, T.A., Burki, F., 2021. A molecular timescale for eukaryote evolution with implications for the origin of red algal-derived plastids. Nat. Commun. 12, 1879. https://doi.org/10.1038/s41467-021-22044-z.
Strother, P.K., Wellman, C.H., 2021. The Nonesuch Formation Lagerstätte: a rare window into freshwater life one billion years ago. J. Geol. Soc. 178, 1–12.
Su, W., 2016. Revision of the Mesoproterozoic chronostratigraphic subdivision both of North China and Yangtze Cratons and the relevant issues. Earth Sci. Front. 23, 156–185.
Sun, W., Wang, G., Zhou, B., 1986. Macroscopic worm-like body fossils from the upper Precambrian (900–700 Ma), Huainan district, Anhui, China and their stratigraphic and evolutionary significance. Precambrian Res. 31, 377–403.
Tang, Q., Pang, K., Xiao, S., Yuan, X., Ou, Z., Wan, B., 2013. Organic-walled microfossils from the early Neoproterozoic Liulaobei Formation in the Huainan region of North China and their biostratigraphic significance. Precambrian Res. 236, 157–181.
Tang, Q., Pang, K., Yuan, X.L., Wan, B., Xiao, S.H., 2015. Organic-walled microfossils from the Tonian Gouhou Formation, Huaibei region, North China Craton, and their biostratigraphic implications. Precambrian Res. 266, 296–318.
Tang, Q., Hughes, N.C., McKenzie, N.R., Myrow, P.M., Xiao, S., Wang, Y., 2017. Late Mesoproterozoic-early Neoproterozoic organic-walled microfossils from the Madhubani Group of the Ganga Valley, northern India. Palaeontology 60, 869–891.
Tang, Q., Pang, K., Yuan, X., Xiao, S., 2020. A one-billion-year-old multicellular chlorophyte. Nat. Ecol. Evol. 4, 543–549.
Tang, Q., Pang, K., Li, G., Chen, L., Yuan, X., Xiao, S., 2021. One-billion-year-old epibionts highlight symbiotic ecological interactions in early eukaryote evolution. Gondwana Res. 97, 22–33.
Teyssèdre, B., 2003. *Chuaria*, *Tawuia*, *Longfengshania*. Trois classes de fossiles précambriens pour un même taxon. C. R. Palevol. 2, 503–508.
Vidal, G., Ford, T.D., 1985. Microbiotas from the late Proterozoic Chuar Group (northern Arizona) and Uinta Mountain Group (Utah) and their chronostratigraphic implications. Precambrian Res. 28, 349–389.
Vorob'eva, N.G., Sergeev, V.N., Petrov, P.Y., 2015. Kotuikan Formation assemblage: a diverse organic-walled microbiota in the Mesoproterozoic Anabar succession, northern Siberia. Precambrian Res. 256, 201–222.
Wan, B., Tang, Q., Pang, K., Wang, X., Bao, Z., Meng, F., Zhou, C., Yuan, X., Hua, H., Xiao, S., 2019. Repositioning the Great Unconformity at the southeastern margin of the North China Craton. Precambrian Res. 324, 1–17.
Wellman, C.H., Strother, P.K., 2015. The terrestrial biota prior to the origin of land plants (embryophytes): a review of the evidence. Palaeontology 58, 601–627.
Xiao, S., Shen, B., Tang, Q., Kaufman, A.J., Yuan, X., Li, J., Qian, M., 2014. Biostratigraphic and chemostratigraphic constraints on the age of early Neoproterozoic carbonate successions in North China. Precambrian Res. 246, 208–225.
Xiao, S., Tang, Q., 2018. After the boring billion and before the freezing millions: evolutionary patterns and innovations in the Tonian Period. Emerg. Top. Life Sci. 2, 161–171.
Xiao, S., Knoll, A.H., Kaufman, A.J., Yin, L., Zhang, Y., 1997. Neoproterozoic fossils in Mesoproterozoic rocks? Chemostratigraphic resolution of a biostratigraphic conundrum from the North China Platform. Precambrian Res. 84, 197–220.
Xing, Y., Liu, G., 1973. Sinian micropalaeophyte assemblages in Yanliao area and its geological significance. Journal of Geology 1–52 [in Chinese].
Yang, E.C., Boo, S.M., Bhattacharya, D., Saunders, G.W., Knoll, A.H., Fredericq, S., Graf, L., Yoon, H.S., 2016. Divergence time estimates and the evolution of major lineages in the florideophyte red algae. Sci. Rep. 6, 21361.
Yang, D., Xu, W., Xu, Y., Wang, Q., Pei, F., Wang, F., 2012. U-Pb ages and Hf isotope data from detrital zircons in the Neoproterozoic sandstones of northern Jiangsu and southern Liaoning Provinces, China: Implications for the Late Precambrian evolution of the southeastern North China Craton. Precambrian Res. 216, 162–176.
Ye, Q., Tong, J., Pang, K., Tian, L., Hu, J., An, Z., 2020. Fossils or sedimentary structures? Carbonaceous spheroids from the shale of the Cryogenian Nantuo Formation in Shengnongjia area. South China. Precambrian Res. 345, 105759 https://doi.org/10.1016/j.precamres.2020.105759.
Yin, L., 1983. Micropalaeophyte assemblages in Diaoyutai Formation and Liulaobei Formation of late Precambrian in North China. Bulletin of Nanjing Institute of Geology and Palaeontology, Chinese Academy of Sciences 6, 9–25 [in Chinese].
Yin, L., 1997. Acanthomorphic acritarchs from Meso-Neoproterozoic shales of the Ruyang Group, Shanxi. China. Rev. Palaeobot. Palynol. 98, 15–25.
Yin, L., Meng, F., Kong, F., Niu, C., 2020. Microfossils from the Paleoproterozoic Hutuo Group, Shanxi, North China: Early evidence for eukaryotic metabolism. Precambrian Res. 342, 105650.
Yin, L., Sun, W., 1994. Microbiota from the Neoproterozoic Liulaobei Formation in the Huainan region, northern Anhui. China. Precambrian Res. 65, 95–114.
Yin, L., 1980. Late Precambrian microfossils from the Diaoyutai Formation, eastern Liaoning, China, *in* Nanjing Institute of Geology and Palaeontology (ed.), Papers for the International Palynological Conference, p. 1–18.
Yochelson, E.L., Fedonkin, M.A., 2000. A new tissue-grade organism 1.5 billion years old from Montana. Proc. Biol. Soc. Wash. 113, 843–847.
Yoon, H.S., Zuccarello, G.C., Bhattacharya, D., 2010. Evolutionary history and taxonomy of red algae. *in* (editors Seckbach, J. and Chapman J.D.) Red Algae in the Genomic Age, Springer Dordrecht Heidelberg London New York, 25–42.
Yoon, H.S., Hackett, J.D., Ciniglia, C., Pinto, G., Bhattacharya, D., 2004. A molecular timeline for the origin of photosynthetic eukaryotes. Mol. Biol. Evol. 21, 809–818.
Zhang, S., Cao, R., Lan, Z., Li, Z., Zhao, Z., Wan, B., Guan, C., Yuan, X., 2022. SIMS Pb-Pb dating of phosphates in the Proterozoic strata of SE North China Craton: Constraints on eukaryote evolution. Precambrian Res. 371, 106562 https://doi.org/10.1016/j.precamres.2022.106562.
Zhang, W., Liu, F., Liu, C., 2020. Detrital zircon U-Pb ages of the late Mesoproterozoic-Neoproterozoic Qiaotou Formation in the Liao-Ji area of the North China Craton: implications for Rodinia reconstruction. Int. Geol. Rev. 63, 1311–1330.
Zhang, W., Liu, F., Liu, C., 2021b. Provenance transition from the North China Craton to the Grenvillian orogeny-related source: Evidence from late Mesoproterozoic-early Neoproterozoic strata in the Liao-Ji area. Precambrian Res. 362, 106281 https://doi.org/10.1016/j.precamres.2021.106281.
Zhang, Z., Peng, P., Feng, L., Gong, Z., Mitchell, R.N., Li, Y., 2021c. Oldest-known Neoproterozoic carbon isotope excursion: Earlier onset of Neoproterozoic carbon cycle volatility. Gondwana Res. 94, 1–11.
Zhang, S., Zhao, Y., Ye, H., Hu, G., 2016. Early Neoproterozoic emplacement of the diabase sill swarms in the Liaodong Peninsula and pre-magmatic uplift of the southeastern North China Craton. Precambrian Res. 272, 203–225.
Zhang, S., Su, J., Ma, S., Wang, H., Wang, X., He, K., Wang, H., Canfield, D.E., 2021a. Eukaryotic red and green algae populated the tropical ocean 1400 million years ago. Precambrian Res. 357, 106166.
Zhao, H., Zhang, S., Ding, J., Chang, L., Ren, Q., Li, H., Yang, T., Wu, H., 2019. New geochronologic and paleomagnetic results from early Neoproterozoic mafic sills and late Mesoproterozoic to early Neoproterozoic successions in the eastern North China Craton, and implications for the reconstruction of Rodinia. GSA Bulletin 132, 739–766.
Zhu, S., Zhu, M., Knoll, A.H., Yin, Z., Zhao, F., Sun, S., Qu, Y., Shi, M., Liu, H., 2016. Decimetre-scale multicellular eukaryotes from the 1.56-billion-year-old Gaoyuzhuang Formation in North China. Nat. Commun. 7, 11500.
Zumberge, J.A., Rocher, D., Love, G.D., 2019. Free and kerogen-bound biomarkers from late Tonian sedimentary rocks record abundant eukaryotes in mid-Neoproterozoic marine communities. Geobiology 18, 326–347.